Synthesis and Characterization of Sn-doped CeS_2 Nanoparticles and their Composites with Graphene Oxide for Application in Supercapacitors

A Dissertation Submitted to the Department of Chemistry, Quaid-i-Azam University, Islamabad in partial fulfillment of the requirement for the degree of

Master of Philosophy

in

Physical Chemistry

by

Wahid Ullah

Department of Chemistry

Quaid-i-Azam University, Islamabad

2018

DECLARATION

This is to certify that this dissertation entitled **"Synthesis and Characterization of Sn-doped CeS Nanoparticles and their Composites with Graphene Oxide for Applications in Super Capacitors"** submitted by ***Mr. Wahid Ullah,*** is accepted in its present form by the Department of Chemistry, Quaid-i-Azam University, Islamabad, as satisfying the dissertation requirements for the degree of ***Master of Philosophy in Physical Chemistry.***

External Examiner:

Dr. Hafiz-ur-Rehman
Principal Scientific Officer
Dr. A.Q. Khan Research Laboratories,
P.O. Box No. 502
Rawalpindi.

Supervisor:

Dr. Syed Mujtaba Shah
Department of Chemistry
Quaid-i-Azam University
Islamabad

Head of Section:

Dr. Hazrat Hussain
Department of Chemistry
Quaid-i-Azam University
Islamabad

Chairman:

Prof. Dr. Shahid Hameed
Department of Chemistry
Quaid-i-Azam University
Islamabad

In the name of Allah, the most beneficent the most Merciful.

"He grants Hikmah to whom He pleases, and he, to whom Hikmah is granted is indeed granted abundant good. But none remember (will receive admonition) except men of understanding."

(Al-BAZARAH:269)

"O Allah, I ask Thee for Beneficial Knowledge, acceptable action, and good provision."

(Al-Tirmidhi Hadith 2487)

Dedicated

to

My Mother (Rest in peace)

All that I am, or hope to be, I owe to my Angel Mother who was a strong and gentle soul, taught me to trust in Allah, believe in hard work and build self-confidence.

My Sisters

A sister is a gift to the heart, a friend to the spirit, and a golden thread to the meaning of life.

My Brothers

Who have always supported me morally and financially.

Acknowledgements

Allah has elevated the degrees those who have believed and those who were given knowledge among you. (Al-Qur'an, 11.58).

All my thanks and gratitude's are for the One, The Everlasting, **Almighty Allah**, the most compassionate, the most beneficent and ever merciful, who gave me the power to do, the sight to observe and mind to think and judge.

This work is a synergistic product of many minds. I am grateful for the inspiration, knowledge and wisdom of all the thinkers who enabled me to put pen to paper, among them are my parents, all my respected teachers and friends who deserve first mention in this dissertation.

A deep sense of gratitude and appreciation is extended to ever affectionate my research supervisor **Dr. Syed Mujtaba Shah** and Co-supervisor **Dr Iqbal Ahmed (AIOU)** for their sincere cooperation and constant encouragement throughout the hard way of research work.

I am highly thankful to **Prof. Dr. Shahid Hameed** Chairman Department of Chemistry Quaid-i-Azam University Islamabad for his kind behavior, encouragement and providing me the necessary instruments for research work in proper time. My special thanks to Head of physical section, **Dr. Hazrat Hussain**, a man of bright wisdom and distinguished character for his kindness.

I would like to acknowledge my seniors and lab fellows **Naveed Ullah, Zarba Dilber Muhammad Nasir Hussain, Rotaba Ansir, Fatma Ayaz, Naimat Ullah, Dr. Abid Ali, Sidra,** and to my ever-supporting friends **Kashif Khan Dawar, Raza Ullah Wazir, Gohar Ayub Khan, Mohsin Afzal Khan Dawar, Shakir Wazir, Tufail Dawar, Sohail Ahmed khan, Er Khalil Dawar, Er Zafar Ayub, Dr Nizam Ud Din, Salah Ud Din, Rehmat Ullah Rahi, Basheer Marwat, my beloved students** for their support.

Wahid Ullah
Wahid.khan1900@gmail.com

Table of Contents

List of Figures

List of Tables

List of Scheme

Abbreviations and acronyms

Abbreviations	Acronyms
C	Capacitance
CeS	Cerium sulphide
CNTs	Carbon nanotubes
Csp	Specific capacitance
CV	Cyclic voltammetry
E	Energy
EDLC	Electrical double layer capacitor
Eq	Equivalent
FTIR	Fourier transformed infrared spectroscopy
FWHM	Full width full maximum
GCD	Galvanostatic charging/discharging
GO	Graphene oxide
Mn	Manganese
MS	Metal Sulphide
MWCNTs	Multiwall carbon nanotubes
NF	Nickle foam
P	Phosphorous
PC	Pseudocapacitor
S	Sulphur

ABSTRACT

Graphene oxide (GO) was prepared by using modified hummer method followed by synthesis of nanoparticles of CeS_2, $CeSnS_2$, $CeSnS_2$/GO, CeS_2/GO via hydro-thermal process. The characterization of the prepared materials was performed by using XRD and FTIR. The results were found in accordance with literature values establishing their successful synthesis. The XRD results showed the presence of hexagonal structure of GO and Orthorhombic structure of CeS_2 nanoparticles. FTIR analysis was done to check the presence of respective functional groups. The electrochemical characterization was done by using the cyclic voltammetry technique where the quasi reversible phenomenon was observed on the surface of the electrode. CV and GDC helped to find out various parameters for capacitance, energy density, current density and power density which confirmed the use of the synthesized materials in energy devices as viable candidates. The comparison of obtained data showed that doping could enhance the electrical and ionic conducting ability of capacity, energy density and power density. The $Ce_{0.55}Sn_{0.45}S$/NF gives excellent specific capacitance of 808.57Fg^{-1} at the scan rate of 10mV/s. CeS_2/NF shows 33.21Wh/kg energy density and 250W/kg power density at current density of 0.1A/g. ($Ce_{0.55}Sn_{0.45}S$/GO)/NF Composites behavior show more closely to electric double layer capacitor. Sn-doping increases the ionic and electronic conducting behavior of CeS_2 nanoparticles.

Key Words: Supercapacitor, nanoparticles, Energy density and capacitance.

CHAPTER-01 INTRODUCTION

1.1 Capacitors

It is an electrochemical device, which consist of two plates (electrodes) separated through some dielectric materials. It is also known as Conventional or electrostatic capacitor. The figure **1.1** shows that when an external voltage is applied, opposite charges start motion towards opposite charge electrodes (positive charges towards negative electrode and negative charges towards positive electrode) and accumulates on their surfaces. These two electrodes which are separated through dielectric layer generate an electric field, which allow the capacitor to store electric charge[1]. The resulting electric field allows the device to store energy. Generally, capacitors are important for its fast release of energy[2]. However, they are unable to store energy for a long time. The important attribute of capacitor is to store electric charge is called its capacitance[3].

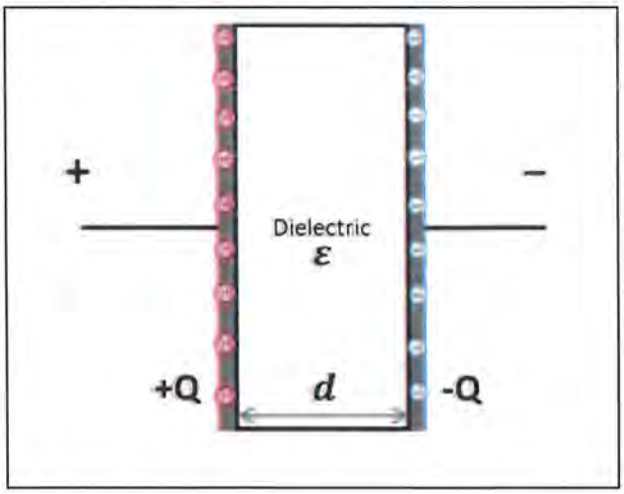

Figure 1.1 *Schematic of an electrostatic capacitor(Reproduced[4])*

1.1.1 Capacitance

The capability of a capacitor to store charge is called capacitance of the capacitor

OR

The ratio of charges to external voltage is called capacitance;

$$Q = CV \quad \text{.....Equation 1.1}$$

C is called the capacitance of the capacitor which is inversely related to the separation between the electrodes and directly on the surface area of the electrodes. Mathematically it can be written as following[5].

$$C = \varepsilon \frac{A}{D} \quad \text{..... Equation 1.2}$$

ε is the constant of proportionality. Known as permittivity constant of the medium between plates.

There are two main attributes of the capacitors, power density and energy density. To measure any one of these, they can be determined as quantities per unit volume or per unit mass. Mathematically the energy can be represented as[6]:

$$E = \frac{1}{2} CV^2 \quad \text{..... Equation 1.3}$$

It is shown from the equation that energy is directly proportional to the capacitance of the capacitor. To calculate the power density, we need the time taken to discharge the capacitor completely. Mathematically power can be written as[6]

$$P = \frac{dE}{dt} \quad \text{..... Equation 1.4}$$

Internal materials of the capacitor like electrodes, dielectric materials and current collectors combinedly contribute to resistance, which is combinedly known as ESR (equivalent series resistance). during the discharge voltage is measured by this resistance. The power of the capacitor is represented as[7]

$$P_{max} = \frac{V2}{4 \times ESR} \quad \text{..... Equation 1.5}$$

The above equation shows the relationship between the power and ESR. Power is inversely dependent on ESR. it is clearly shown from the equation that how the P_{max} is limiting due to ESR. Generally, the capacitors have relatively higher power density (even higher than 5000 Wkg^{-1}). However, energy density is lower (0.01 -0.05 Wh/kg).

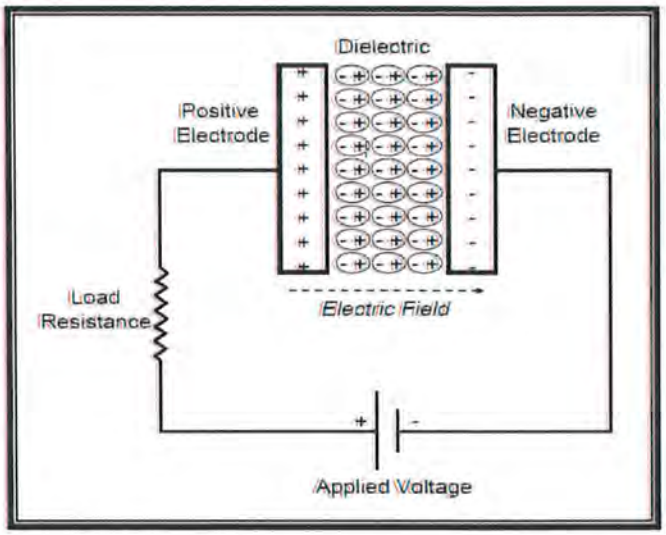

Figure 1.2 *Schematic diagram of a capacitor((Reproduced [8])*

1.2 Supercapacitors

Supercapacitors are energy storage devices, which are also known as electrochemical capacitors or ultracapacitors. Supercapacitors achieve capacitances several times larger than conventional capacitors by utilizing thin electrolytic dielectrics and high surface area of materials of electrodes[9-10]. Due to this reason supercapacitors are capable to store greater energy densities. As shown in the **figure 1.3** Like conventional capacitors supercapacitors also consist of two electrodes. which are highly porous. these electrodes are dipped in an electrolytic solution and are separated through a dielectric medium. This medium or layer is permeable for charges to pass through[11]. When the voltage from external source is applied to supercapacitor, opposite charges moves toward opposite electrodes (positive towards negative and negative towards positive) and accumulate on the surface of electrodes. Ions passes through the dielectric membrane and adsorb into the pores of electrodes. The electrodes don't allow the recombination of the ions. Two layers of charges formed at each of the electrode[10] . High surface area and high porosity for the materials of electrodes is desired to get higher energy density. Thin membrane is used as a dielectric separator. In this way we can improve the energy and capacitance dramatically. In addition to this, we can maintain a considerable higher power density with a lower ESR (equivalent series resistance) value which is comparable with general capacitors. Supercapacitors are mainly divided in 3 types[12]. Which are discussed below.

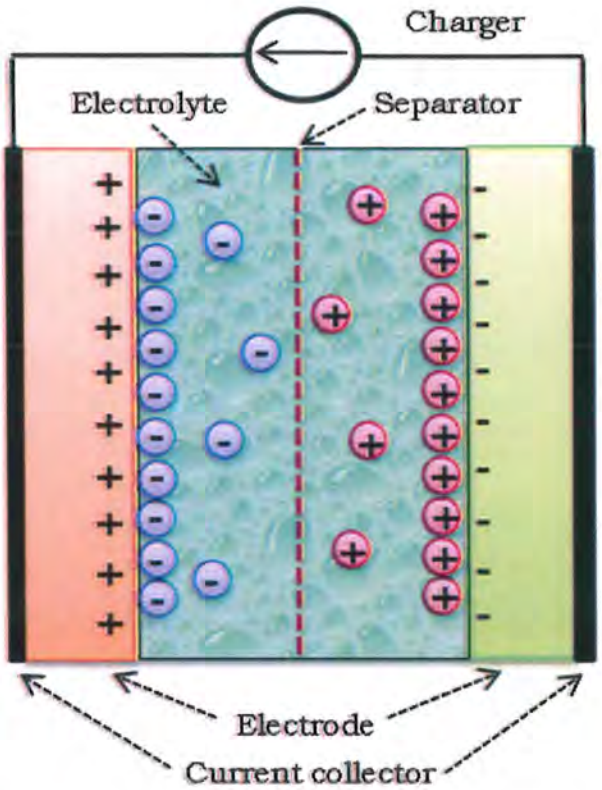

Figure 1.3 *schematic diagram of Supercapacitor((Reproduced [13])*

1.3 Electrochemical Double-Layer Capacitors

Such type of capacitor has two electrodes (carbon based), filter and an electrolyte. Like conventional capacitors, they store charge non-faradaically. No redox reactions occur. Energy store in the form of electrical double layer (charges). When external source of voltage is applied, opposite charges move towards their respective electrodes. Due to the attraction of unlike charges ions defuse into the pores of the electrodes from electrolytic solution through separator[14]. However, the recombination of charged particles is prevented by the electrodes. So, two layers of charges formed. A decrease in the separation of electrodes contributes with double layers to achieve higher energy density. The performance of the device can be controlled by adjusting the nature of materials of the electrodes. An organic or aqueous electrolyte can be used in EDLCs. Such as KOH, H_2SO_4 have generally low ESR than organic electrolytes. e.g. acetonitrile[15]. A detailed comparison between electrolytes is beyond of this work. The classes of EDLC can be distinguished by their electrode materials. Generally, the electrode materials of carbon exhibit higher surface area, low cost, and more ecofriendly fabrication techniques comparatively [16].

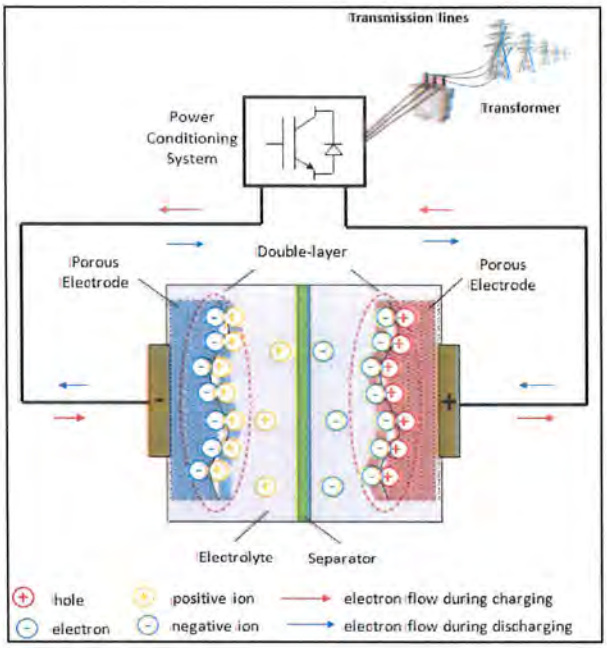

Figure 1.4 *Electrical double layer capacitor(Reproduced [17])*

1.4 Pseudocapacitor

Unlike to EDLCs, that store charge non-faradaically, pseudocapacitor stores the charges through the redox reactions between electrolytes and the electrodes. Such type of behavior is termed as faradaic behavior. This is done by electro sorption, redox reactions. The redox reactions may Contribute with pseudocapacitor to achieve greater energy densities and specific capacitance than EDLCs[18]. Two electrode materials are being used in pseudocapacitor for storing charges. They are metal oxides and conducting polymers[19].

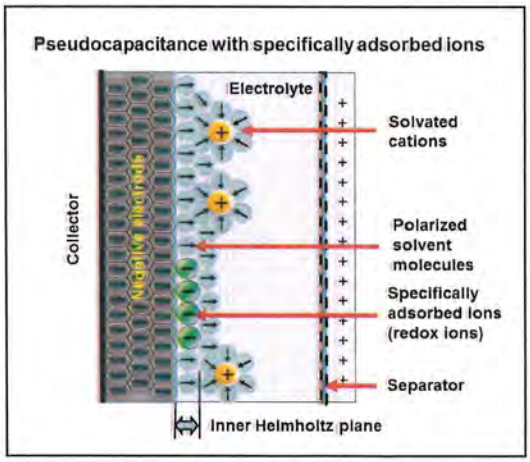

Figure 1.5 *Pseudocapacitance*

1.5 Hybrid capacitors

Hybrid capacitors act as a bridge between pseudo capacitors and EDLCs. Because hybrid capacitor store charge both electrostatically and faradaically. It is to exploit both the relative merits and demerits of pseudocapacitors and EDLCs. That's why their power and energy densities are relatively greater than EDLCs. Affordability and cycling stability are the limitations of EDLCs[20-21]. These limitations degrade the EDLCs in comparison to hybrid capacitors. Three main types of hybrid capacitors are differentiated by their electrode materials. Asymmetric, battery type and composites[22].

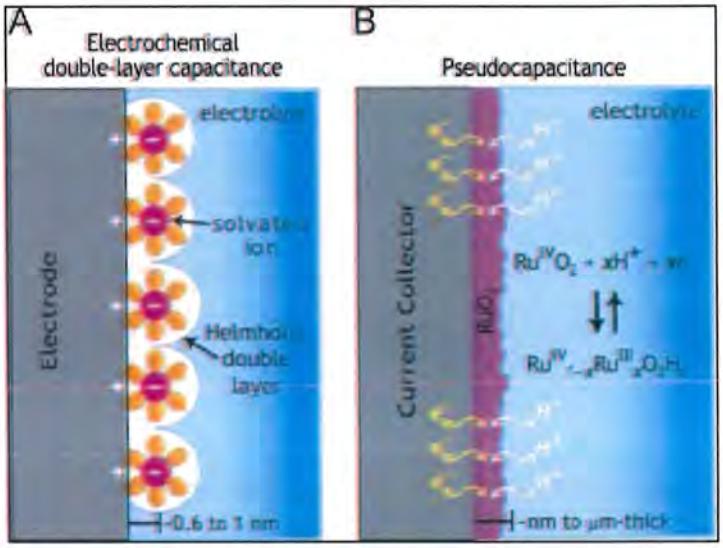

Figure 1.6 *Hybrid capacitor(Reproduced [23])*

1.6 Batteries

Batteries are most common power sources for different applications in industrial and consumer electronics. Battery is an electronic device that converts stored chemical energy into electrical energy through special chemical reaction. A general battery consists of single or more electrochemical cells. Each complete cell comprises two electrodes. These two electrodes are connected electrically by an electrolyte with positive and negative charged ions[24]. By the transport of anions and cations the polarity of the cell can be identified. During the process of charging, the electrode with negative ions transport is known as anode, while the electrode with positive ions transport is known as cathode[25-26].

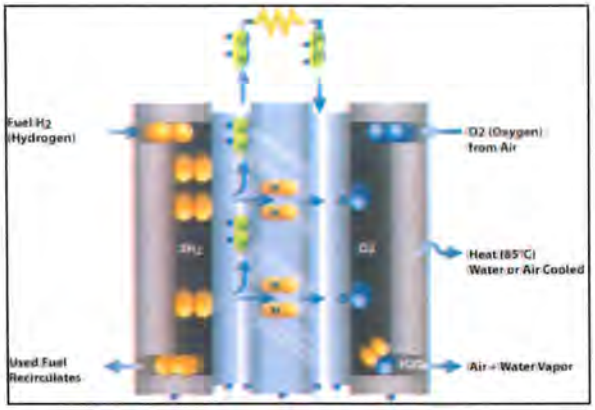

Figure 1.7 *The mechanisms by which battery works(Reproduced [27])*

1.6.1 Types of Batteries

Batteries are divided into two groups. Disposable batteries and rechargeable batteries. Disposable batteries are designed to irreversibly convert the chemical energy into electrical energy. On the other hand, the rechargeable batteries can restore the original composition with charging process (e.g. lead acid, nickel metal hydride (NiMH), nickel-zinc (NiZn), nickel-cadmium (NiCd), and lithium-ion cells). It is concluded that, disposable batteries have higher energy density than rechargeable batteries[28].

Lithium-ion batteries represent the best electrochemical cells with a high energy density of 120-170 Wh/kg, moderate weight and no memory effect as well. In spite of their high specific energy, the lithium-ion batteries and their substitutes are characterized by low charge-discharge rates or low power density[29].

The anode of a commercial lithium-ion cell is composed of graphite or other carbon materials. Typically, the cathode material is lithium intercalated compounds like iron phosphate, cobalt oxide, manganese oxide, and nickel oxides. The lithium ions can migrate into and away from both electrodes. During the charging process, the lithium ions move into the graphite anode. In the discharge process, when connected to an external load, the ions migrate back to the cathode. The lithium ion is highly reactive and can react with water in the electrolyte forming hydrogen gas and lithium hydroxide. Thus, the organic e and a well-sealed packaging method are employed in lithium ion batteries to minimize the possibility of dangerous reactions[30-31].

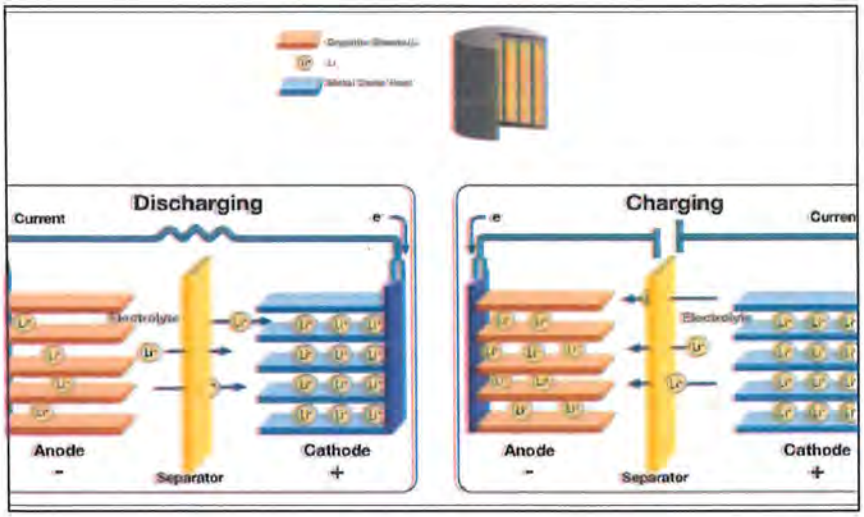

Figure 1.8 *charge/discharge mechanisms of a lithium ion battery(Reproduced [33])*

1.7 Comparison among electrochemical energy storage devices

Figure 1.8 shows the easy approach to differentiate between the performance of various energy storage devices. It is also called the Ragone chart. Dash lines represent the total time required for charging and discharging the device. From the figure below, it is shown that as compare to fuel cells and batteries the conventional capacitors have relatively higher power density, but a very lower energy density. It indicates that the conventional capacitor requires very short time to charge or discharge and generates very high power, the capacitors cannot store much energy in unit mass. Fuel cells and batteries can store much more energy, but their dynamic performances are very weak. The power density of supercapacitors is more than that of battery[34]. Charging and discharging of supercapacitors is rapid and can maintain a considerable high energy density[35]. For such reasons, supercapacitors have significant advantages in peak power delivery applications, like electric vehicles acceleration, regenerative braking, and steady power supply. Supercapacitors bridge the power gap between batteries and capacitors and also hold number of other important properties[36]. No chemical change occurs during the charge storing process as it is a physical process. Therefore, it is highly reversible and have a huge number of charge discharge cycles, up to 1 million times[37].

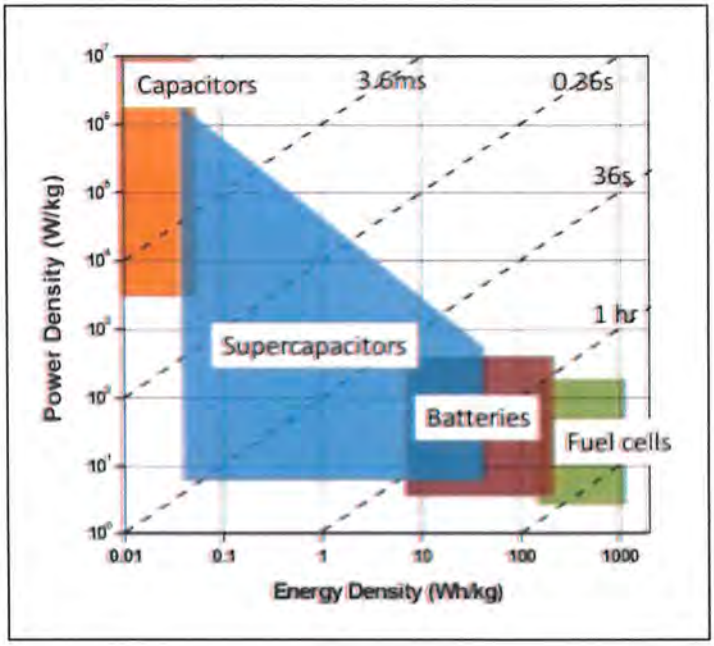

Figure 1.9 *comparison among different storage devices(Reproduced [38])*

1.8 Nanoparticles

Nanoparticles are also known as Nanoclusters, Nano Powder or Nanocrystals. These are microscopic particles, having one dimension less than 100 nm[39]. Due to its vast variety of applications in different fields such as biomedical, optical and electronic, Nanoparticle become one of the most important area in scientific research[40]. Nanoparticles have a numerous scientific influence because they made a bridge between molecular or atomic structure and bulk materials. A bulk material with irrespective of its size should have perpetual physical properties, but it is not frequently the case at nano-scale. Properties of size-dependent have been observed in semiconductors for example quantum confinement etc, surface plasmon resonance in some metal particles and in magnetic particles the superparamagnetic properties[41].

As the size of the materials approach to nanoscale, their properties change as the percentage of atoms become significant at the outer surface of the materials. More than one micrometer for bulk materials the percentage of atoms become lower at surface of elements comparative to the whole number of atoms of the materials. Nanoparticles demonstrating many distinct properties which are comparative to bulk element.

For example, about the scale of 50 nm movement of copper cluster/atoms, occurring the bend of bulk copper (ribbon, wire etc.)[42].

Less than 50 nm of nanoparticle of copper have super hard materials that don't exhibit the properties like malleability and ductility like bulk copper. Continuously alteration in properties is not needed. Using thermal energy of room temperature magnetization pathway can switch by ferroelectric element having size less than 50 nm[43]. Nanoparticle suspension is possible due to solvent interaction with particle surface, this result for the materials neither to float nor sink in liquid. Nanoparticles are smaller enough to produce a quantum effect and to restrain their electron. Due to this reason their visible properties are often unexpected. For example, in solution the appearance of gold nanoparticle is black from deep red. As compare to volume ratio nanoparticles have very high surface area. This provides a high drive force for diffusion, particularly at increased temperatures. The melting point of nanoparticles also reduce by high surface area to volume ratio[44].

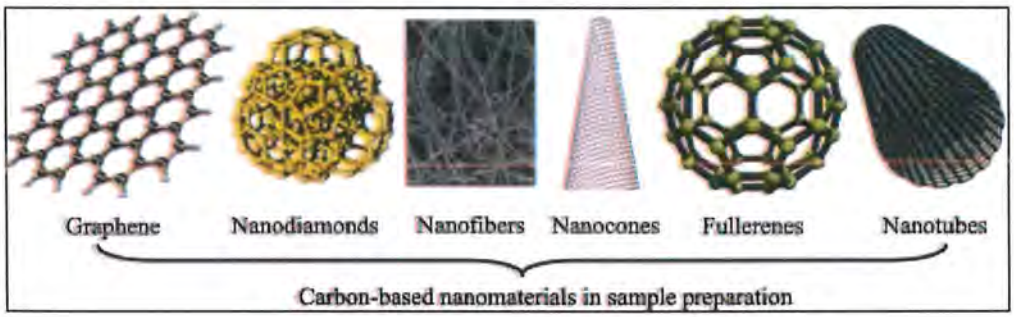

Figure 1.10 *Carbon based nanoparticles*

1.9 Nanocomposites

Those composites in which at least one phase shows dimension in nanometer range (1 nm = 10^{-9} m)[45]. Nanocomposites are suitable materials that overcome the limitations of monolithic and micro composites. Nanocomposites have been reported in 21st century having property of combination and design uniqueness which were not present in the conventional composites. The overall understanding of these properties yet to be reached, even though in 1992 the first inference was reported on them.[46] The change in particle properties has been reported and can be observed also, and when the size of particle is less than a particular level than it is called critical size[47]. Moreover, at interface phase interaction enhanced because the dimension reached to nanometer level. Carbon nanotubes (CNTs) discovered in 1991. By

constructing their composites with other nanoparticles shown unique electrical[48], thermal and mechanical properties. This area added an interesting and new dimension [49]. Utilizing CNTs as textiles[10] and composite products made further inroads for the application and processing of CNT-containing nanomaterials. Currently a business occasions and new technology offer by nanocomposites for the entire segment of industry to make it environmentally friendly[50].

1.10 Metal sulfide

In comparison to active materials which are used for Pseudocapacitor show higher conductivity such as hydroxide, transition metal oxides, metal Sulphides and their composites support a high-speed electron movement in electrodes and contribute even to a loading material which are highly active to specific capacitance. With high electronic conductivity most of the metal Sulphides are semiconductors[51]. Some are characterized as electronic conductors[52](e.g., Ni_3S_2). Additionally, a higher capacitive performance is shown by binary and tertiary Sulphides as compared to single component Sulphides because of higher electronic conductivities and their richer redox reactions resulting from the binary and ternary metal ions synergistic effect[53]. This thesis has a detailed discussion about the application of cerium Sulphides, tin doped cerium Sulphides and their composites with GO in supercapacitors applications[54-55].

2 Method and materials

2.1 Chemicals used

Chemicals which were used in the preparation of CeS_2, Tin doped CeS_2, Graphene oxide and nanocomposites of CeS_2, Tin Dopes CeS_2 with GO are given in the table below. Their names, molecular formulas and company names are mentioned in the following table.

Table 2.1 *Different chemicals used*

Sr. No	Compounds	Chemical Formula	Supplier
1	Cerium Nitrate hexahydrate	$Ce(NO_3)_3.9H_2O$	BDH AnalaR ®
2	Sodium Sulfide ninehydrated	$NaS_2.9H_2O$	ARUNI-CHEM ®
3	Tin chloride dihydrate	$SnCl_4.2H_2O$	Merck ®
4	Potassium per magnate	$KMnO_4$	BDH AnalaR ®
5	Sulfuric Acid	H_2SO_4	BDH AnalaR ®
6	Powder graphite	C	Sigma-Aldrich ®
7	Nitric Acid	HNO_3	BDH AnalaR ®

2.2 Synthesis Procedures

2.2.1 Synthesis of Cerium Sulphide nanoparticles through hydrothermal method

15 ml of Cerium Nitrate hexahydrate solution (0.1 M) was mixed with 15 ml of Sodium Sulphide (0.2 M) Solution. The mixture was stirred through magnetic stirrer at room temperature for 15 minutes. After this it was transferred into autoclave of 50 ml capacity. The autoclave was placed in furnace for 14 hrs under 200 °C temperature. Then the reaction

mixture was removed, centrifugated and was washed with distilled water. The product was dried at 60 °C for 5 hrs in oven[56]. Final Product was obtained and was powdered.

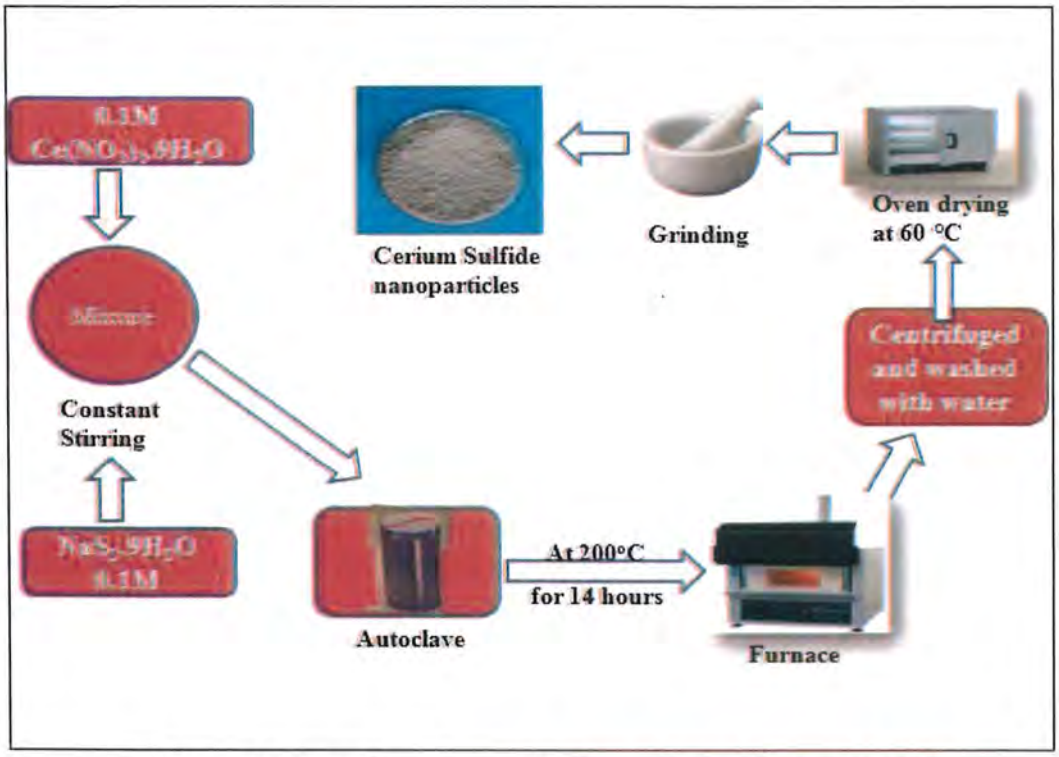

Scheme 2.1 *Flow sheet diagram for the synthesis of Cerium Sulphide*

2.2.2 Synthesis of the Tin Doped Cerium Sulphide nanoparticles by hydrothermal method

The same procedure was followed for Sn doped CeS_2 as for the synthesis of CeS_2[56-57]. but 6.75 ml of Cerium Nitrate nine hydrate added instead of 15 ml. Tin acetate tetrahydrate solution (0.1 M) was added in the mixture of Cerium nitrate and sodium Sulphide solutions. Onward the procedure was same as for CeS_2 synthesis.

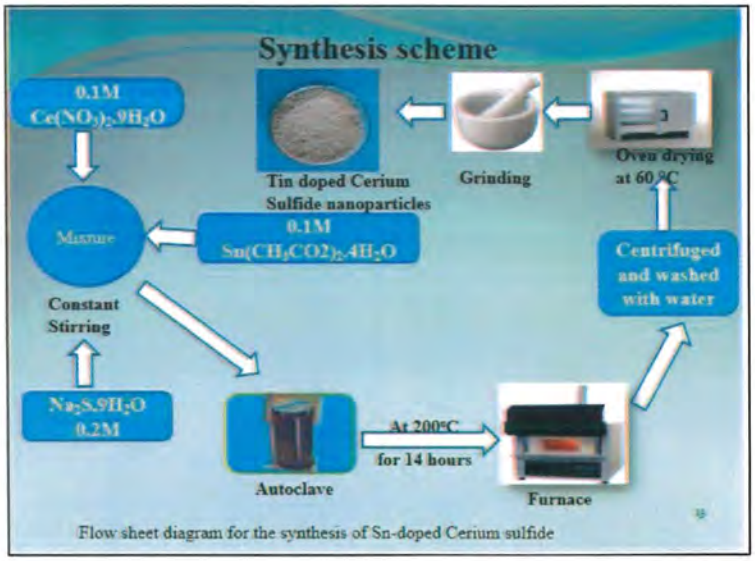

Scheme 2.2 *Flow sheet diagram for the synthesis of tin doped* CeS_2

2.2.3 Synthesis of expanded graphite

14 g of powdered graphite were taken in a beaker. 30 ml of each of HNO_3 and H_2SO_4 was added. The mixture was stirred continuously for 15 min and then was kept for 3 days in the locker. After 3 days 800 ml of distilled water was added and then was centrifuged at 4500 rpm for 20 min. The product was dried at 60 °C for 3 hrs. The final product was expanded Graphite[58, 59-60].

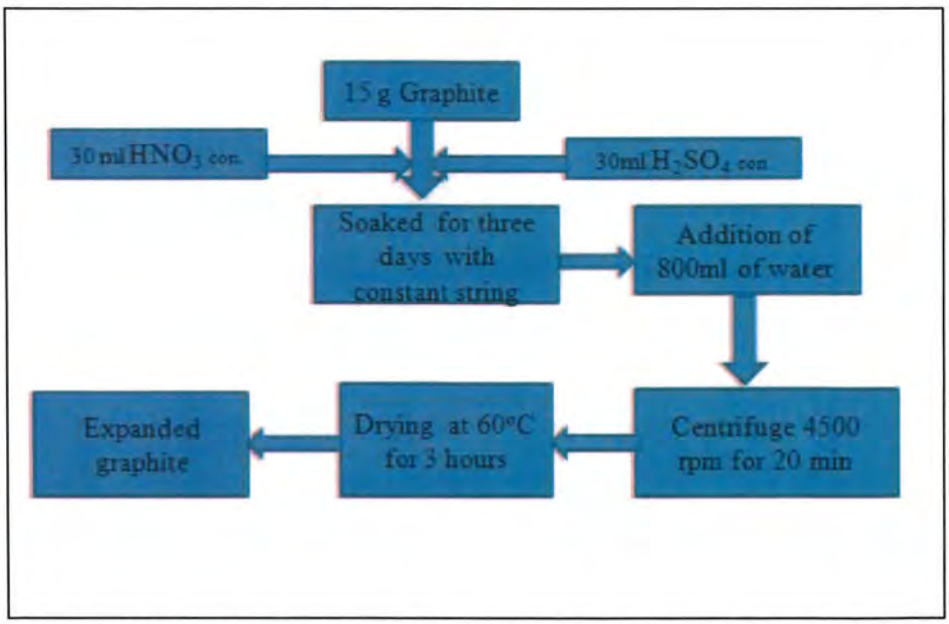

Scheme 2.3 *Flow sheet diagram for the preparation of expanded graphite*

2.2.4 Graphene oxide synthesis

Graphene oxide (GO) nanoparticles were synthesized through modified hummer method [4]. 4 g of expanded graphite was taken in a beaker and 75 ml of concentrated H_2SO_4 was added. It was stirred for 2 hrs in ice bath. After this, 12 grams of $KMnO_4$ was added. Again for 2 hrs in ice bath the mixture was continuously stirred at temperature below 35 °C. After this the reaction mixture was transferred to water bath and 375 ml of distilled water were added. Temperature was raised up to 90 °C for 3 hrs with continuous stirring. Furthermore, 300 ml of distilled water was added and stirred for 2 hrs at room temperature as. The final reaction mixture was centrifuged and then dried at 60 °C for 2 hrs. The final product was known as GO.

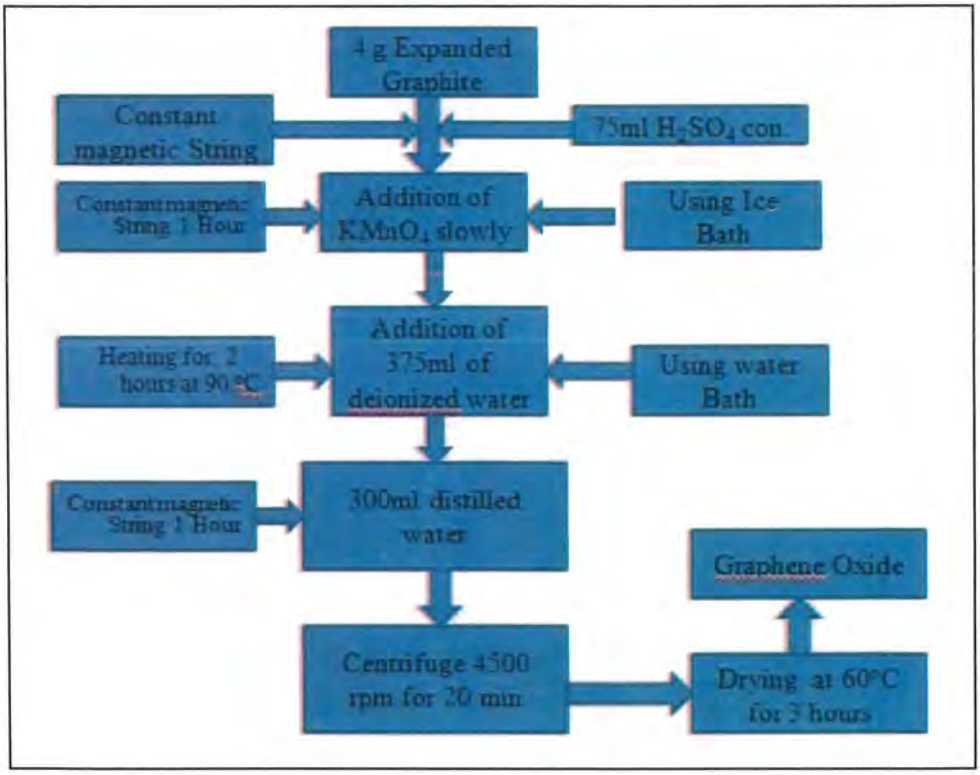

Scheme 2.4 *Flow sheet diagram for the preparation of Graphene Oxide (modified hummar method)*

2.2.5 Hydrothermal Synthesis of CeS_2/GO and Sn doped CeS_2/GO nanocomposites

Nanocomposites of doped and undoped nanoparticles of CeS_2 with GO were prepared through hydrothermal method. Particular amount of nanoparticles and Graphene oxide were

taken in 1:1 ratio by mass for composites formation. 15 ml of both of Cerium Nitrate hexahydrate and Sodium Sulfide ninehydrated solution were $_{taken}$ in a beaker having molarity 0.1 M and 0.2 M respectively. 0.432 g of GO was added to this mixture and was sonicated for 10 minutes. Then the reaction was shifted to autoclave. The autoclave was placed in a furnace at 200 °C for 14 hrs. The product was washed several times with distilled water and was centrifuged. The nanoparticles were dried in oven at 60 °C for 6 hrs. The final product was obtained CeS_2/GO nanocomposite. The same procedure was followed for Sn doped CeS_2 but instead of 15 ml of Cerium Nitrate, it was added 6.75 ml. and Tin Acetate tetra hydrated solution was added. Molarity was 0.1M. In the last step 0.385 grams GO was added for Sn doped CeS_2/GO nanocomposites. The final product was obtained $Ce_{0.55}SnS_2$/GO.

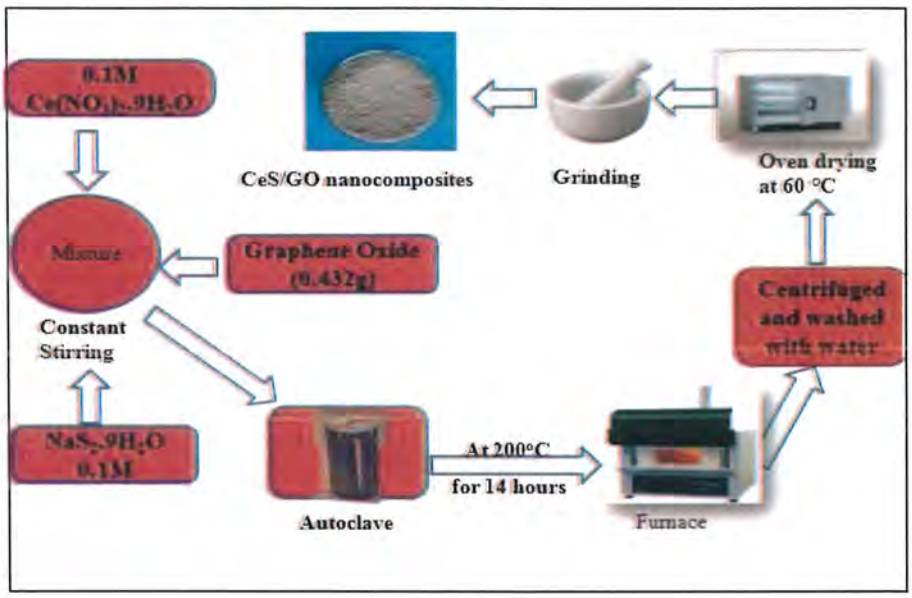

Scheme 2.5 *Flow sheet diagram for the synthesis of Cerium sulfide /GO*

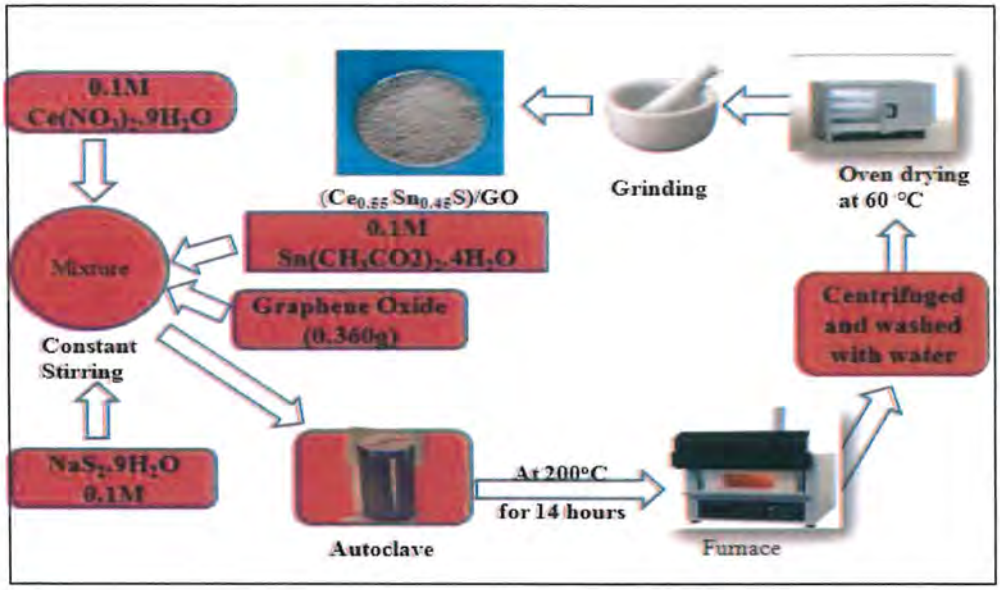

Scheme 2.6 *Flow sheet diagram for the synthesis of Sn-doped Cerium Sulphide /GO*

2.2.6 Preparation of working electrode

A small strip of Nickle foam was taken. To remove its contamination, it was washed and sonicated 3 times in distilled water. After the distilled water it was rewashed with acetone. The clean and pure nickel foam was dried in oven. 10mg nanoparticles were sonicated in a separate beaker in absolute alcohol[61]. 1 to 2 drops of nafion was put on the nickel foam and then the mixture of nanoparticles was added drop wise on nickel foam. The electrode was dried for 24 hrs at room temperature and was called modified working electrode.

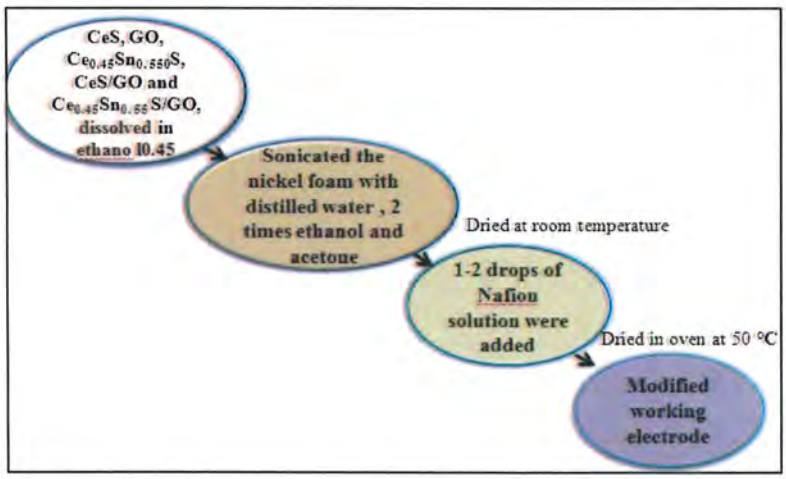

Scheme 2.7 *Electrode Modification Process*

2.3 Instruments used

2.3.1 Ultraviolet-Visible Spectroscopy

Molecular spectroscopy that includes investigation of the interaction of Ultra violet (UV) - Visible radiation with particles. Ultra violet and visible radiations have enough energy to cause an electronic Excitation starting from filled orbital into the next higher Energy unfilled orbital. At this point an electron absorb light of a required wavelength and excited to a higher energy molecular orbital[62].

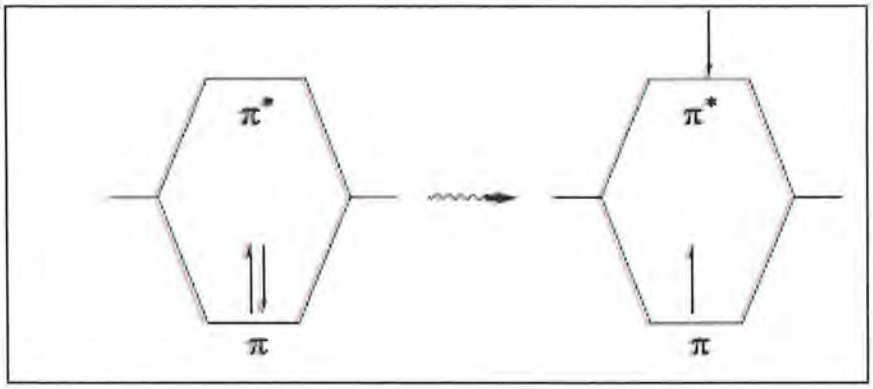

Figure 2.1 *π to π* excitation*

UV-Visible Spectroscopy falls in the range between 200-400nm and 400-800nm relates to the Visible area. Selection rules or transaction rules contains specific transition of atoms starting with one quantum state then onto the another and furthermore tell us concerning whether a particular transition is permitted or forbidden[63].

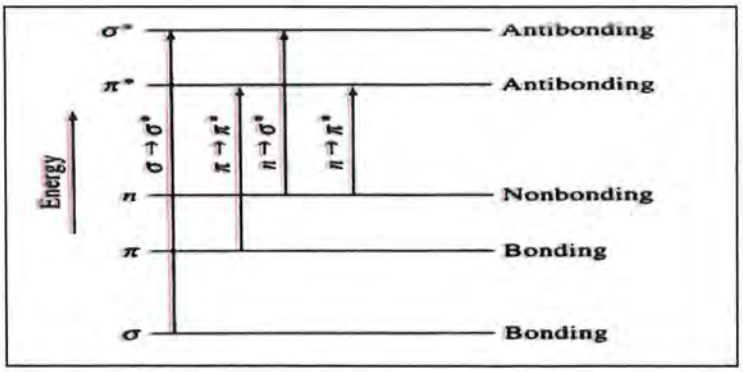

Figure 2.2 *Possible Electronic transition of n, δ and π electrons*

Figure 2.3 *Experimental setup UV−Vis Spectrometer*

UV-Visible spectroscopy makes utilization of Beer-Lambert law in which absorbance of a chemical species is associated with its concentration. Molar absorptivity coefficient is the qualities of absorbing specie which depend upon the nature of concentration species and its interaction with a medium with which the chemical species interface. Relation of absorbance of a compound with its concentration is given by the accompanying condition given beneath.

$$A = \varepsilon cl \quad \text{..... Equation 2.1}$$

Where A represent to absorbance of incident electromagnetic radiation, ε represent to the molar absorptivity coefficient, c represent to concentration of absorbing specie and l is the way length of cuvette[64].

2.3.2 Cyclic Voltammetry

To study the electrochemical properties of a compound, Cyclic voltammetry (CV) is performed as the main experimental technique. CV can also be performed for natural biological material or an electrode surface. Through cyclic voltammetry redox reactions can be clearly observed. That's why it has given prime importance[65].

2.3.2.1 Basics of cyclic voltammetry

CV consists of a working electrode and reference electrode. the working electrode is dipped in the solution and determine the estimating current. The potential of this electrode is controlled over a reference electrode, for example silver/silver chloride cathode (Ag/AgCl)[66].

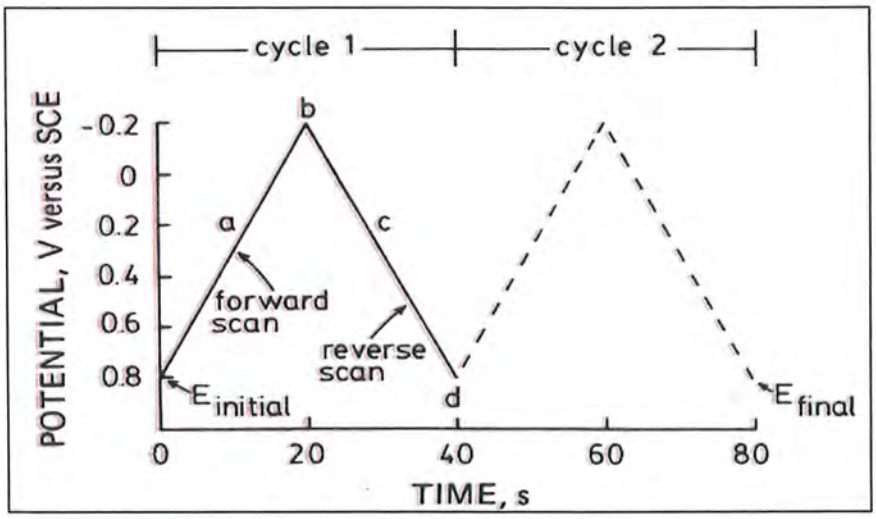

Figure 2.4. *Typical excitation signals for cyclic voltammetry*[67]

The controlling potential which is connected over these two cathodes can he considered an excitation signal. The excitation signal for CV is a linear potential sweep with a triangular waveform as shown in **Figure 2.4**

Following is the experimental set up for cyclic voltammetry

Figure 2.5 *Experimental setup of Cyclic Voltammeter*

2.3.3. XRD technique

This is as a brief introduction to some of the common X-ray diffraction spectroscopy utilized as a materials characterization. It's used for the determination of crystallinity of the material and for the crystallite size of the material[68].

2.3.3.1 Instrument and estimating principle of XRD Spectroscopy

XRD analysis depends on constructive interference of monochromatic X-rays and a crystalline sample: The cathode beam tube produces X-beams, and then filtered to produce the monochromatic radiations. The radiations are directed to focus on materials (sample). When the interactions of incident beams occur with the sample, Constructive interference is produced. When the conditions satisfy Bragg's Law ($2d\sin\theta = n\lambda$)[69]. This correlates the wavelength of EMR to the angle of diffraction, the cross section dividing in a crystalline sample.

Figure 2.6 *Experimental setup of XRD Spectroscopy*

2.3.4 FT-IR Spectroscopy

FTIR (Fourier Transform Infra-red Spectroscopy) is a delicate method specially to identify organic chemicals substances in an entire scope of uses despite the fact that it can likewise characterize some inorganics. For example, incorporate paints, adhesives, pitches, polymers, coatings and drugs. Through This instrument we can isolate and characterize an organic contamination.

In FTIR spectrophotometry matter interact with electromagnetic radiation in InfraRed region. In this region the molecular vibration couples with the radiations. By absorbing IR radiations molecules become excited into higher energy states. The absorption in this region is correspondent to the bonds present in the molecules. The frequency range is estimated as 4000 – 600 cm-1 wave number[70].

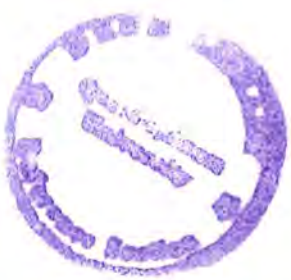

Figure 2.7 *Experimental setup of FT-IR Spectroscopy*

3.1: XRD analysis

Figure 1 shows the XRD patterns of graphene oxide (GO), CeS_2 and Sn-doped CeS_2 and their nanocomposites with graphene oxide. GO shows only one peak at 9.853 of 2θ which conform the synthesis of GO nanoparticles no other peak is observed related to other particles such as graphite, reduce graphene oxide, etc. which shows the purity[71]. The average crystallite size of GO was 53nm as calculated by Scherrer formula. XRD pattern showed that CeS_2 and Ce_2S_3 both phases formed simultaneously.30.1221°, 35.4467°, 43.2184°, 53.6492°, 57.1455° and 62.7049° and accredited to miller indexes 100, 111, 230, 220, 301 and 460 respectively. The average crystallite size was 20nm calculated by Scherrer formula. In Sn-doped cerium sulfide other peaks also appeared due to doping. Nanocomposites did not show peak of GO at 9.854°. In literature it showed that the diffraction peak would become weak or disappeared if the regular stacks of graphite or graphene oxide were destroyed by exfoliation. So, when CeS_2 was coated on the surface of Graphene oxide nanosheets, the regular stacks of graphene oxide were vanished completely.

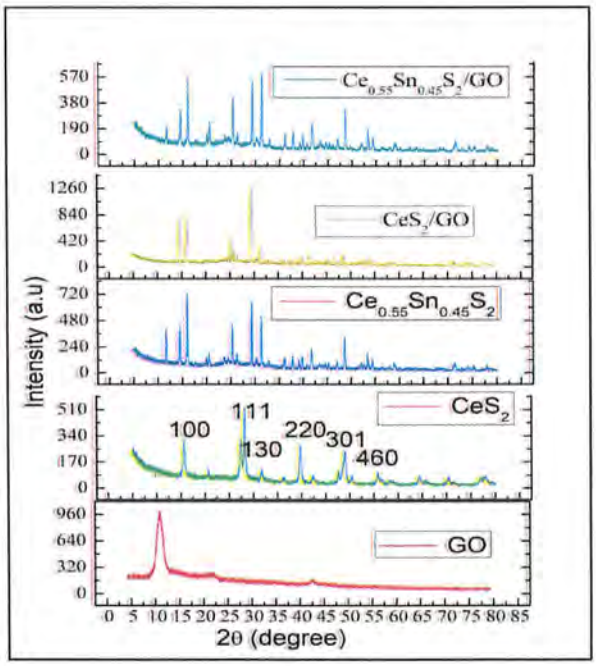

***Figure 3.1** XRD pattern of GO, CeS_2, $Ce_{0.55}Sn_{0.45}S_2$, CeS_2/GO and $Ce_{0.55}Sn_{0.45}S$/GO*

The XRD pattern in the **figure.3.1** shows the successful synthesis of CeS_2 nanoparticles. The hkl values were compared with the values given in the standard ICSD card no 01-075-1109 and were well matched. This suggested orthorhombic structure of the CeS_2.

The figure also shows the XRD pattern of CeS_2 nanocomposite with GO. Their characteristic peaks show successful formation of nanocomposites materials.

3.2 FT-IR analysis

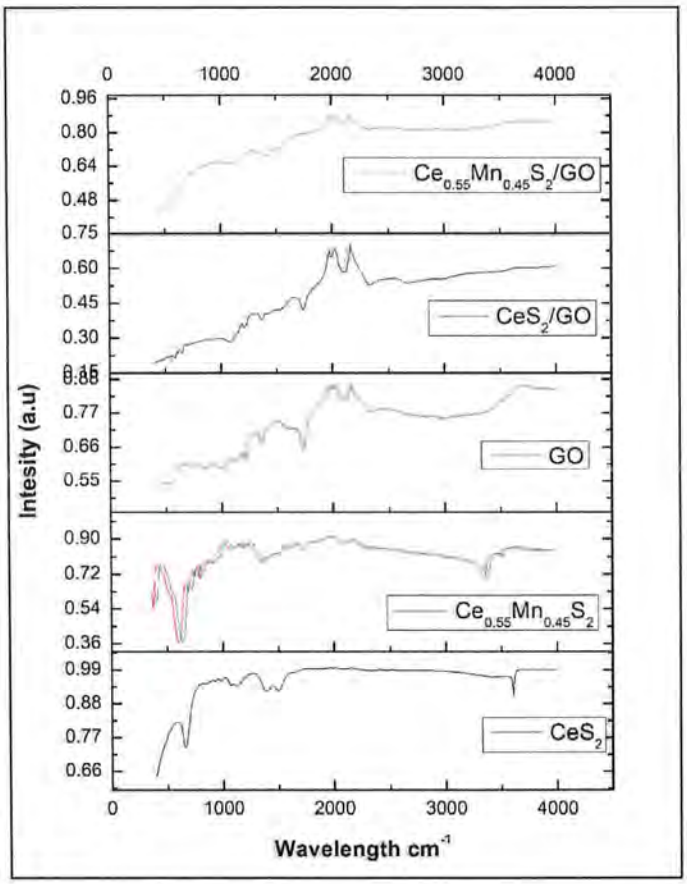

***Figure 3.2** FTIR spectra of GO, CeS_2, $Ce_{0.55}Sn_{0.45}S_2$, CeS_2/GO and $Ce_{0.55}Sn_{0.45}S$/GO*

Figure 3.2 shows the FT-IR spectra for CeS_2, $Ce_{0.55}Sn_{0.45}S$, GO, CeS_2/GO and $Ce_{0.55}Sn_{0.45}S$/GO their composites with GO. The main characteristic absorption of infrared radiations by graphene oxide indicates the presence of oxygen-containing functional groups on the surface of GO located at 1612.90 cm^{-1} (C=C), 1731.68cm^{-1} (C=O), 1028.99 cm^{-1} (C–O–C), 1362.45 cm^{-1} (C-OH). The absorption peak in the range of 3600-3100cm^{-1} attributed to –OH group of water adsorbed by the samples[72-74]. Another weak absorption band at 1633cm^{-1}

was assigned to the scissoring mode of water molecules adsorbed on the surface of the material. The band at 500cm^{-1} corresponds to the Ce-O stretching vibration. The weak band at round 850cm^{-1} is ascribed to metal-sulfur bonding.

3.3 Cyclic Voltammetry

3.3.1 Cyclic Voltammetry of CeS_2

Cyclic voltammogram (CV) for CeS_2 in 0.1M KOH over a voltage window of 0 V to 0.75 V was obtained. Scan rate was 0.03 Vs^{-1} and Ag/AgCl was used as a reference electrode. A pronounced deviation from the ideality has shown in voltammogram.

Curve deviated from rectangular type because of reversible redox reaction on the surface of active materials of CeS nanoparticles of nickel foam electrode. Two peaks have been observed in the Voltammogram. One is at negative side showing the reduction of Ce and the other at positive side showing the oxidation of Ce. The materials of electrodes shown pseudocapacitive behavior[75]. The redox reactions in the voltammogram proved the reversibility of the materials[76].

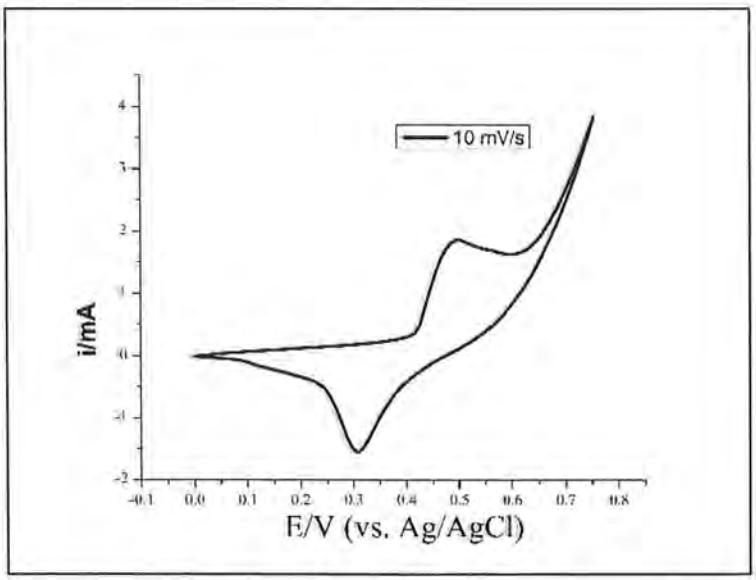

Figure 3.3 *Cyclic voltammogram of Cerium sulfide at constant scan rate (0.03 Vs^{-1})*

3.3.2 Cyclic Voltammetry of $Ce_{0.55}Sn_{0.45}S_2$

Cyclic voltammogram (CV) for $Ce_{0.55}Sn_{0.45}S_2$ in 0.1M KOH over a voltage window of 0 V to 0.75 V was obtained. Scan rate was 0.03 Vs^{-1} and Ag/AgCl was used as a reference electrode. A pronounced deviation from the ideality has shown in voltammogram.

The cyclic voltammogram curve deviated from EDLC type voltammogram because of reversible redox reaction on the surface of active materials of $Ce_{0.55}Sn_{0.45}S_2$ nanoparticles on nickel foam electrode. Only reduction peak was observed in the voltammogram. The oxidation peak disappeared which may be due to the tin doping in the CeS_2 nanoparticles. One negative side showing the reduction of and the at positive side showing the oxidation. The materials of electrodes shown pseudocapacitive behavior. The redox reactions in the voltammogram proved the reversibility of the materials.

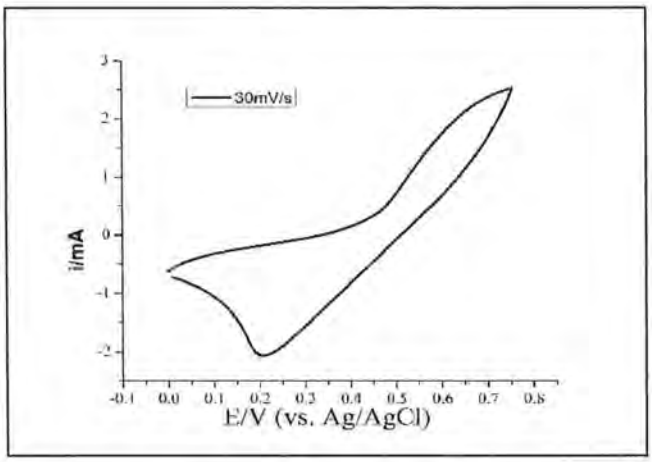

Figure 3.4 *Cyclic voltammogram of $Ce_{0.55}Sn_{0.45}S_2$ at constant scan rate (0.03 Vs^{-1})*

3.3.3 Cyclic Voltammetry of GO

Cyclic voltammogram (CV) for GO in 0.1M KOH over a voltage window of 0 V to 0.75 V was obtained. Scan rate was 0.03 Vs^{-1} and Ag/AgCl was used as a reference electrode. A pronounced deviation from the ideality has shown in voltammogram.

Capacitive behavior of GO nanoparticles on nickel foam electrode deviated from ideal cyclic voltammogram. It was due to reversible redox reaction on the surface of active materials of GO nanoparticles of nickel foam electrode. Two peaks have been observed in the Voltammogram. The oxidation and reduction peaks possibly due to different functional oxygenated functional group on the surface of graphene oxide nanoparticles. Furthermore, voltammogram proved the reversibility of the materials.

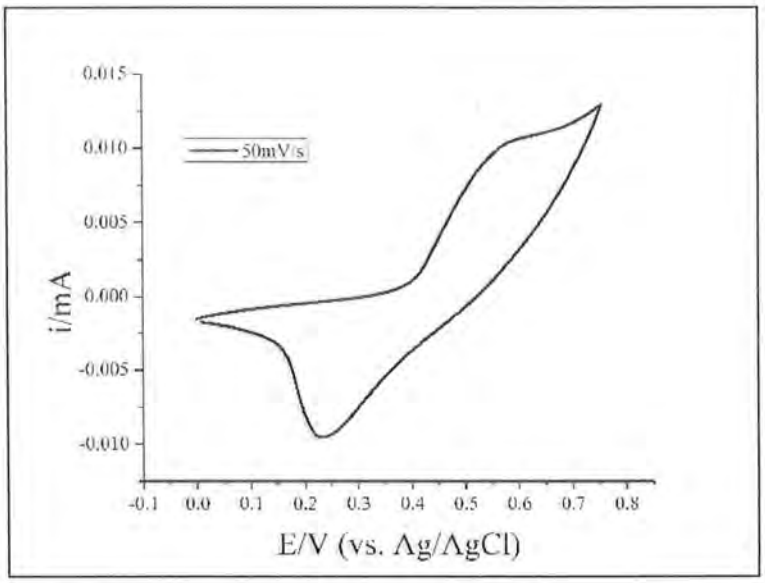

Figure 3.5 *Cyclic voltammogram of GO at constant scan rate (0.05 Vs^{-1})*

3.3.4 Cyclic Voltammetry of CeS_2/GO

Cyclic voltammogram (CV) for CeS_2/GO in 0.1M KOH over the voltage window of 0 V to 0.75 V was obtained. Scan rate was 0.03 Vs^{-1} and Ag/AgCl was used as a reference electrode. A pronounced deviation from the ideality has shown in voltammogram.

The cyclic voltammogram of CeS_2/GO nanocomposites on nickel foam deviated from electrical double layer capacitor because of reversible redox reactions on the surface of active materials of electrode. Here only one peak was observed in cyclic voltammogram. The materials of electrodes have shown pseudocapacitive behavior. The redox reactions in the voltammogram proved the reversibility of the materials.

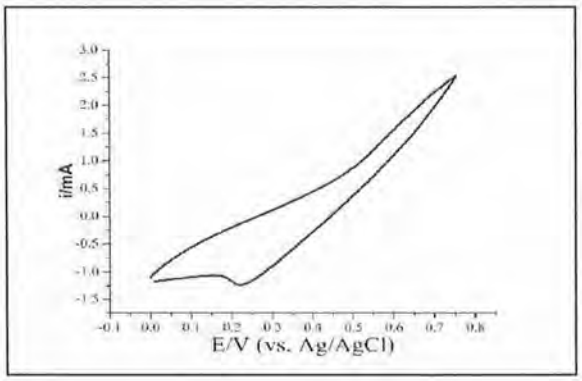

Figure 3.6 *Cyclic voltammogram of CeS_2/GO at constant scan rate (0.05 Vs^{-1})*

3.4 The effect of different Scan rates on Cyclic voltammogram

3.4.1 The effect of different Scan rates on Cyclic voltammogram of CeS_2

As in the figure below, Cyclic voltammetry (CV) for CeS2 in 0.1M KOH was done. voltage window was in the range 0 V to 0.75 V at different scan rates and Ag/AgCl was used as a reference electrode. The changing in scan rate effected the cyclic voltammogram as shown in figure 3.7. When the scan rate was changed from 10mV/s to 100mV/s, Oxidation peak was shifted from 0.45V to 0.534V at scan rates of $10mVs^{-1}$ and 100 mV/s respectively. the oxidation and reduction current also became more positive and more negative when the scan rate increased. Also, (reduction peak) the negative potential was shifted from 0.312V to 0.25V at the scan rates of 10 mV/s and 100 mV/s respectively. It was shown from the voltammogram that the materials of electrodes were stable even at 100 mV/s scan rate. It was also shown that the reaction was reversible. The lower slope at lower scan rate indicates that the anions need more time to diffuse in to the bulk of CeS/NF electrode[77].

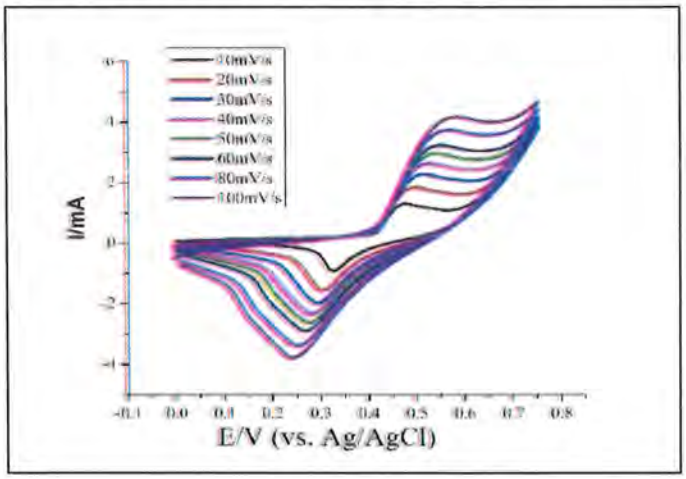

Figure 3.7 *Cyclic voltammogram curves for cerium sulphide nanoparticles at different scan rates*

3.4.2 The effect of different Scan rates on Cyclic voltammogram of $Ce_{0.55}Sn_{0.45}S_2$

As in the figure below, cyclic voltammetry (CV) for $Ce_{0.55}Sn_{0.45}S_2$ in 0.1M KOH was done. voltage window was in the range 0 V to 0.75 V at different scan rates and Ag/AgCl was used as a reference electrode. The oxidation and reduction peaks were shifted to more positive and negative respectively when current density was increased. When the scan rate was changed from 10mV/s to 100mV/s, there is a very slight shift in the oxidation peak. But at the negative potential the shift was more pronounced. It was shifted from 0.25V to 0.20V

at the scan rates of 10 mV/s and 100 mV/s respectively. It was shown from the voltammogram that the materials of electrodes were stable even at 100 mV/s scan rate. It was also shown that the reaction was reversible. The lower slope at lower scan rate indicates that the anions need more time to diffuse in to the bulk of $Ce_{0.55}Sn_{0.45}S_2$/NF electrode. The CV profile showed the that the reaction was reversible and stable event at 100 mV/s as shown in figure 3.8.

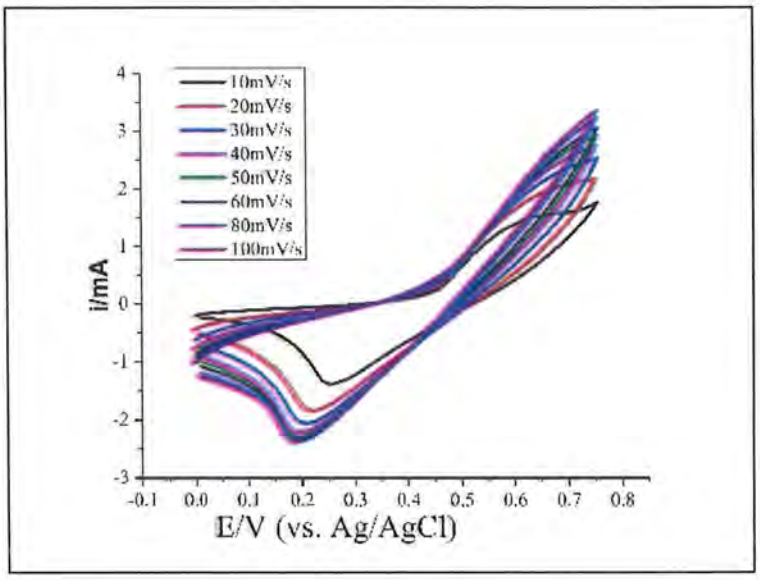

***Figure** 3.8 Cyclic voltammogram curves for $Ce_{0.55}Sn_{0.45}S_2$ nanoparticles at different scan rates*

3.4.3 The effect of different scan rates on cyclic voltammogram of GO

As in the figure below, Cyclic voltammetry (CV) for GO in 0.1M KOH was done. voltage window was in the range 0 V to 0.75 V at different scan rates and Ag/AgCl was used as a reference electrode. The peak of cyclic voltammogram was affected with increasing scan rate. When scan rate increased the oxidation peak shifted from 0.50 to 0.665 V at the scan rate of $10mVs^{-1}$ to$100mVs^{-1}$ respectively. Similarly, the negative potential was shifted from 0.327 to 0.1686 V at the scan rate as used for oxidation of supercapacitor materials. The current measured for cathodic reaction were 3.15, 6.177, 7.84, 9.406, 10.68, 11.73, 13.68 and 15.31 mA at above scan rate. 2.698, 5.084, 6.798, 8.191, 9.53, 10.41, 12.03 and 13.24 mA measured the anodic current at electrode. The electrode materials were found stable even at 100mV/s scan rate and revisable. The small slop at lower scan rate indicates that the lower scan rates allow more time for the anions to access the bulk of the electrode.

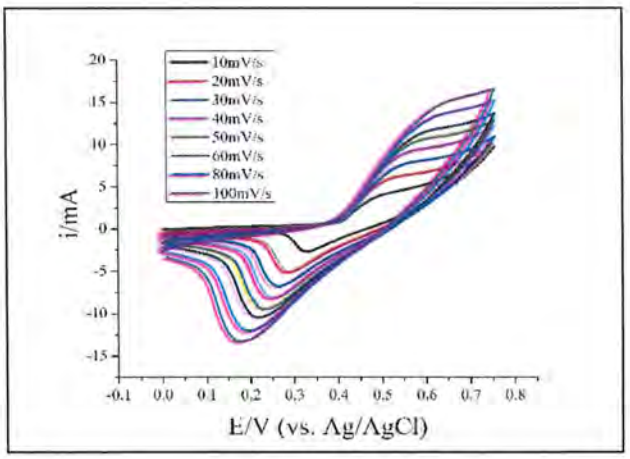

Figure 3.9 *Cyclic voltammogram curves for graphene oxide nanoparticles at different scan rates*

3.4.4 The effect of different Scan rates on Cyclic voltammogram of CeS_2/GO

Figure 3.10 shows Cyclic voltammetry (CV) for CeS2/GO in 0.1M KOH. Voltage window was in the range 0 V to 0.75 V at different scan rates and Ag/AgCl was used as a reference electrode. As the scan rate was changing, peaks were also changing. But as shown from the figure 3.10 there is only the reduction peak at negative potential. Which is shifted from 0.26V to 0.17V at the scan rates of 10 mV/s to 100 mV/s respectively.

It was shown from the voltammogram that the materials of electrodes were stable even at 100 mV/s scan rate. The figure below indicates that the reaction is reversible. The lower slope at lower scan rate indicates that the anions need more time to diffuse in to the bulk of CeS2/GO/NF electrode.

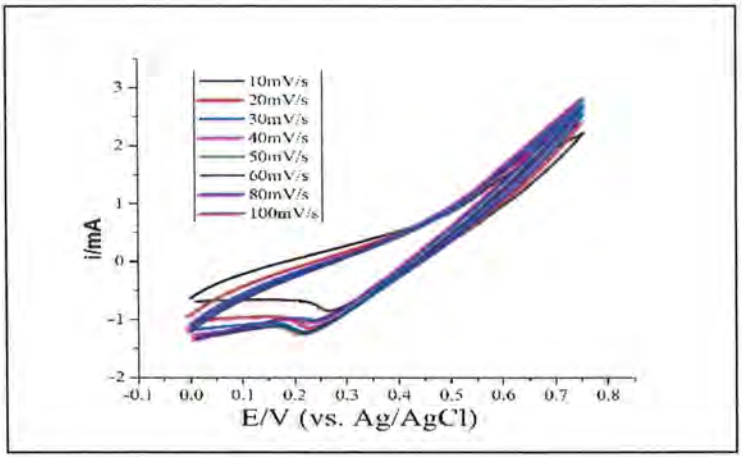

Figure 3.10 *Cyclic voltammogram curves for CeS_2/GO nanoparticles at different scan rates*

3.5 Effect of different scan rates on Specific Capacitance.

3.5.1 Effect of scan rates on Specific Capacitance of CeS_2

Figure 3.11 shows the effect of different scan rates (from 10mV/s to 100mV/s) on specific capacitance of CeS_2 nanoparticles. It is clearly shown in the figure that the specific capacitance is inversely dependent on scan rate for Cerium Sulphide. As the specific capacitance of CeS_2 is decreasing with increasing scan rate. Decreased in specific conductance connected with kinetics of pseudocapacitance reaction and lower electronic conductivity of the Cerium Sulphide nanoparticles[78]. From the figure 3.11 the specific capacitance was calculated as

Table 3.1 *specific capacitance at different scan rates*

Specific capacitance(F/g)	426.3	369.6	335.2	311.3	292	275.3	248.3	224.6
Scan rate(mV/s)	10	20	30	40	50	60	80	100

A highest specific capacitance of ~426.3F/g was observed for CeS_2 at scan rate of 10mV/s. This indicated that the materials of electrode could be used as a supercapacitor material as it can store large amount of electrical charge.

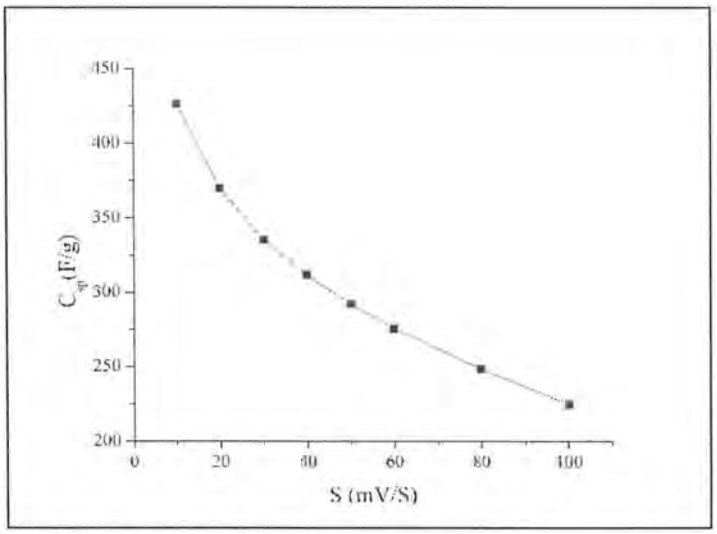

Figure. 3.11 *Change in Specific Capacitance with change in scan rate*

3.5.2 Effect of scan rates on Specific Capacitance of $Ce_{0.55}Sn_{0.45}S_2$

Figure 3.12 shows the effect of different scan rates (from 10mV/s to 100mV/s) on specific capacitance of $Ce_{0.55}Sn_{0.45}S_2$ nanoparticles. It is clearly shown in the figure that the specific capacitance is inversely dependent on scan rate for $Ce_{0.55}Sn_{0.45}S_2$. As the specific capacitance of $Ce_{0.55}Sn_{0.45}S_2$ is decreasing with increasing scan rate. Decreased in specific conductance connected with kinetics of pseudocapacitance reaction and lower electronic conductivity of the $Ce_{0.55}Sn_{0.45}S_2$ nanoparticles. From the **Figure 3.13** the specific capacitance was calculated as

Table 3.2 *specific capacitance at different scan rates for* $Ce_{0.55}Sn_{0.45}S_2$

Scan rate mV/s	10	20	30	40	50	60	80	100
Specific capacitance (Fg^{-1})	463.13	333.2	256.16	205.67	167.64	125.73	98.66	87.32

A highest specific capacitance of ~463F/g was observed for $Ce_{0.55}Sn_{0.45}S_2$ at scan rate of 10mV/s. Specific capacitance has been increased for the doped material as compared to pure CeS_2. This indicated that the materials of electrode could be used as a supercapacitor material as it can store large amount of electrical charge.

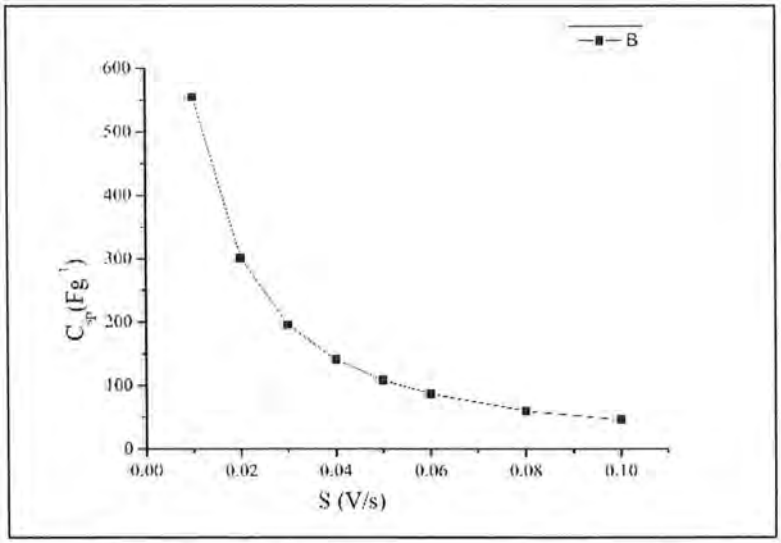

Figure 3.12 *Change in Specific Capacitance with change in Scan rate*

3.5.3 Effect of different scan rates on Specific Capacitance of GO

The effect of scan rate from 10mVs^{-1} to 100 mVs^{-1} on the specific capacitance of CeS_2 is shown in Figure 3.17. It was observed that the specific capacitance of graphene oxide was decreased with increasing scan rate. At higher scans rate reduction in specific capacitance could be related with the kinetics of pseudocapacitance reaction and lower electronic conductivity of the graphene oxide nanoparticles. The specific capacitance was calculated 1160 Fg^{-1}, 1015 Fg^{-1}, 913.33 Fg^{-1}, 825 Fg^{-1}, 782 Fg^{-1}, 715 Fg^{-1}, 609.875 Fg^{-1} and 529 Fg^{-1} at the scan rate of 10mV/s, 20mV/s, 30mV/s, 40mV/s, 50mV/s, 60mV/s, 80mV/s, and 100mV/s respectively. The higher capacitance 1160 F/g was observed at the scan rate 10 mV/s. It proved that graphene oxide can be used for supercapacitor materials.

Table 3.3 *Values of specific capacitance at different scan rates*

Specific capacitance(F/g)	1160	1015	913.33	825	782	715	609.87	529
Scan rate(mV/s)	10	20	30	40	50	60	80	100

The cathodic peak current and anodic peak current measured at different scan rate were plotted versus the square root of a scan rate as shown in Figure 3.18. From the plot, it can be easily deduced that the process is diffusion controlled. The mechanism for the charge storage

was quasi-reversible electrochemical reactions at the surface of the electrode. The mechanisms were deduced from the cathodic and anodic current peaks. Good linear relationships indicated the diffusion-controlled process for graphene oxide /NF electrode.

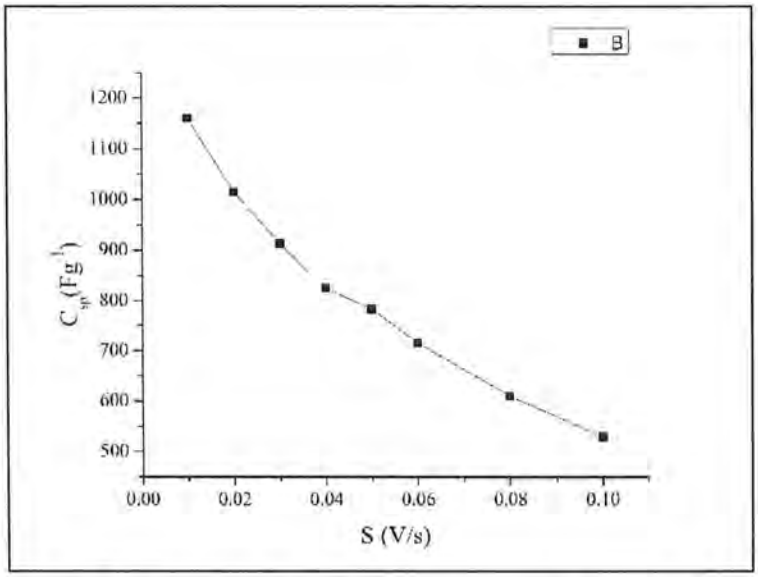

Figure 3.13 *Change in Specific Capacitance with change in Scan rate*

3.5.4 Effect of scan rates on Specific Capacitance for CeS_2/GO

Figure 3.14 shows the effect of different scan rates (from 10mV/s to 100mV/s) on specific capacitance of CeS_2/GO nanoparticles. It is clearly shown in the figure that the specific capacitance is inversely dependent on scan rate for CeS_2/GO. As the specific capacitance of CeS_2/GO is decreasing with increasing scan rate. From the figure 3.16 the specific capacitance was calculated

Table 3.4 *Values of specific capacitance at different scan rates*

Specific capacitance(F/g)	690.4	463.1	333.2	256.1	205.6	167.6	125.7	98.6
Scan rate(mV/s)	10	20	30	40	50	60	80	100

A highest specific capacitance of ~690.4F/g observed for CeS_2/GO at scan rate of 10mV/s. This indicates that the materials of electrode can be used as a supercapacitor material as it can store large amount of electrical charge.

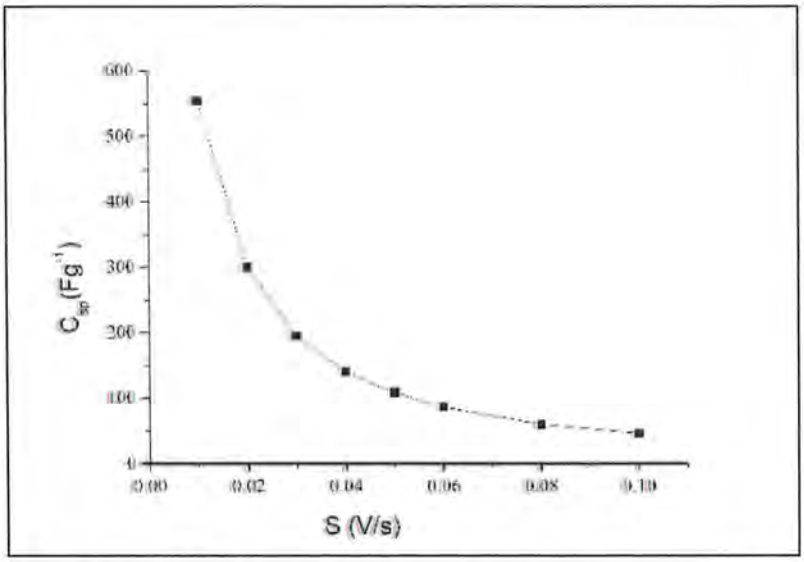

Figure 3.14 *Change in Specific Capacitance with change in Scan rate*

3.6 Energy density and Scan rate

3.6.1 Energy density and Scan rate for CeS_2

the figure below shows that energy density of the material changes with change in the scan rate. It is shown that the energy density was inversely related to scan rate. Energy density is high for lower scan rate.

Table 3.5 *Different values of energy densities at different scan rate*

E (Wh/Kg)	33.21	28.79	26.11	24.25	22.74	21.45	19.34	17.50
Scan rate(mV/s)	10	20	30	40	50	60	80	100

As the scan rate was increased, the specific capacitance was decreased and in turn, the energy density was also decreased. As the specific capacitance and energy density have direct relations. High energy density of 33.21538Wh/Kg was observed at scan rate of 10mV/s, which indicated that high energy density can be stored in the materials. At lower scan rate the Cerium Sulphide nanoparticles have the capability to store more energy but when the scan rate was increased, slope was decreased more. Onward the decrease in slope was less pronounced[79].

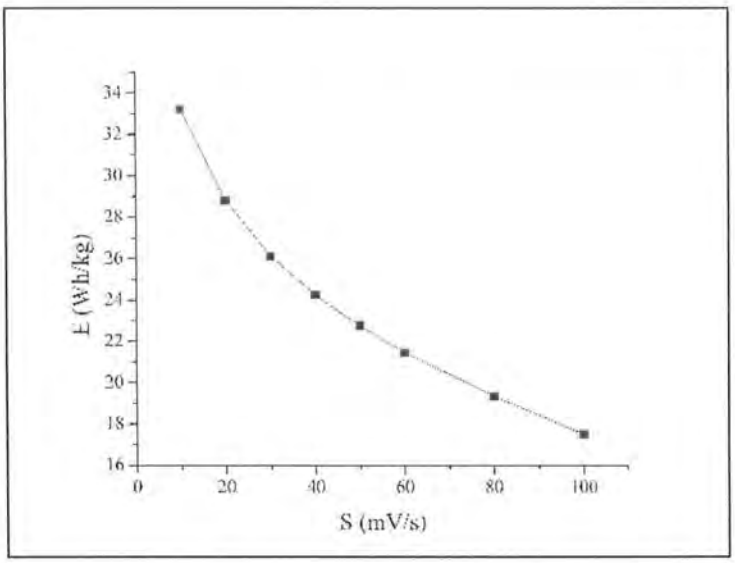

Figure 3.15 Change in Energy density with change in Scan rate for cerium sulfide

3.6.2 Energy density and Scan rate for $Ce_{0.55}Sn_{0.45}S_2$

The figure below shows that energy density of the material changes with change in the scan rate. It is shown that the energy density was inversely related to scan rate. Energy density is high for lower scan rate.

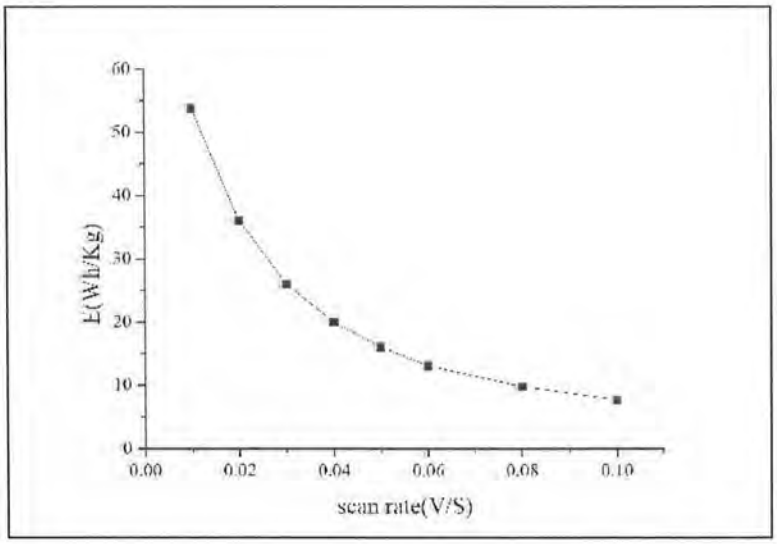

Figure 3.16 Change in Energy density with change in Scan rate for $Ce_{0.55}Sn_{0.45}S_2$

Table 3.6 *Different values of energy densities at different scan rates*

E ($Whkg^{-1}$)	55.2	45.7	34.81	19.4	14.32	10.065	9.62	9.52
S (mV/s)	10	20	30	40	50	60	80	100

As The scan rate was increased, the specific capacitance was decreased and in turn the energy density was also decreased. As the specific capacitance and energy density have direct relations. High energy density of 55.2 Wh/Kg was observed at scan rate of 10mV/s, which indicated that high energy density can be stored in the materials. At lower scan rate the $Ce_{0.55}Sn_{0.45}S_2$ nanoparticles have the capability to store more energy but when the scan rate was increased, slope was decreased more. Onward the decrease in slope was less pronounced.

3.6.3 Energy density and Scan rate for GO

Figure 3.17 shows that energy density of the material changes with change in the scan rate. It is shown that the energy density was inversely related to scan rate. Energy density is high for lower scan rate.

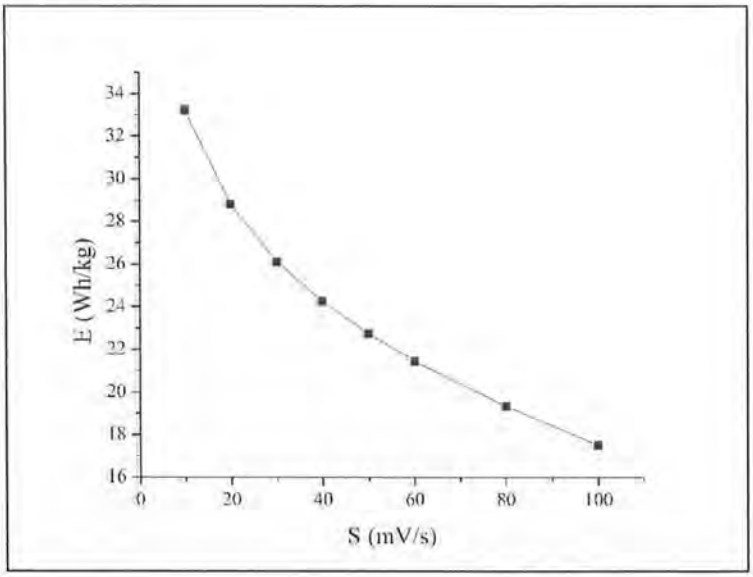

Figure 3.17 *Change in Energy density with change in Scan rate.*

Different values of energy densities at different scan rates are given in the following table

As The scan rate was increased, the specific capacitance was decreased and in turn the energy density was also decreased. As the specific capacitance and energy density have direct relations. High energy density of 90.63Wh/Kg was observed at scan rate of 10mV/s, which indicated that high energy density can be stored in the materials. At lower scan rate the GO nanoparticles have the capability to store more energy but when the scan rate was increased, slope was decreased more. Onward the decrease in slope was less pronounced.

3.6.4 Energy density and Scan rate for CeS_2/GO

It is clearly shown in the figure below that energy density of the material changes with change in the scan rate. It is shown that the energy density was inversely related to scan rate. Energy density is high for lower scan rate.

Table 3.7 *Different values of energy densities at different scan rates*

Energy density ($Whkg^{-1}$)	43	22	16	10	9	8.5	8	7
Scan rate (mV/s)	10	20	30	40	50	60	80	100

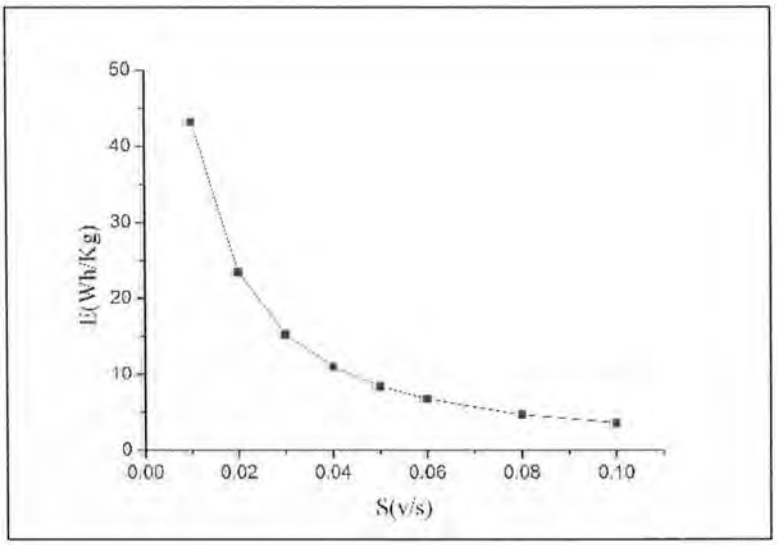

Figure 3.18 *Change in Energy density with change in Scan rate.*

Different values of energy densities at different scan rates are 43Wh/Kg, 22Wh/Kg, 16Wh/Kg, 10Wh/Kg, 9Wh/Kg, 9.5Wh/Kg, 8Wh/Kg at the scan rate of 10 mV/s, 20mV/s, 30mV/s, 40mV/s, 50mV/s, 60mV/s, 80mV/s, and 100mV/s respectively. As The scan rate was increased, the specific capacitance was decreased and in turn the energy density was also decreased. As the specific capacitance and energy density have direct relations. High energy density of 43 Wh/Kg was observed at scan rate of 10mV/s, which indicates that high energy density can be stored in the materials. At lower scan rate the CeS_2/GO nanoparticles have the capability to store more energy but when the scan rate was increased, slope was decreased more. Onward the decrease in slope was less pronounced.

3.7 Galvanostatic charging and Discharging (GCD)

3.7.1 Galvanostatic Charging/Discharging of CeS_2

Figure 3.19 shows the charging and discharging of CeS_2/NF supercapacitor in 0.1M KOH solution at constant current density (2 Ag^{-1}). The procedure was same for galvanostatic charge and discharge as followed for cyclic voltammetry technique. figure 3.19 shows deviation from triangular curve which indicates that the electrode materials have pseudocapacitive behavior. This behavior was due to reversible redox reactions. The current during these reactions is called faradic current. To charge and discharge completely CeS_2/NF materials took 479 seconds and 14 seconds respectively. The materials discharged fully because the total reactions occurred on the surface were not completely reversible. The decrease in discharging time may represent the irreversibility of the materials. In charging curve (upper curve) the peak represent oxidation and in discharging curve the peak is due to reduction. The deviation of the curve also justifies the cyclic voltammogram of the electrode[80].

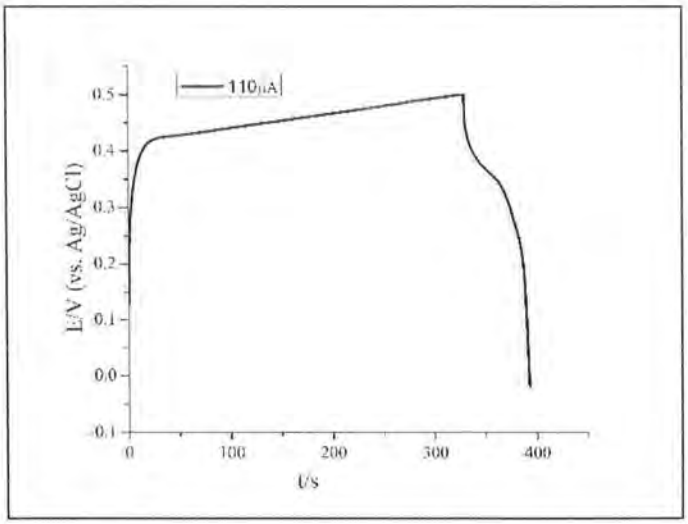

Figure.3.19 *Galvano static charging discharging curves of the CeS_2/NF at 0.2Ag^{-1} current density*

3.7.2 Galvanostatic Charging/Discharging of $Ce_{0.55}Sn_{0.45}S_2$

Figure 3.20 shows the charging and discharging of $Ce_{0.55}Sn_{0.45}S_2$/NF supercapacitor in 0.1M KOH solution at constant current density ($2Ag^{-1}$). The procedure was same for galvanostatic charge and discharge as followed for cyclic voltammetry technique. figure 3.20 shows deviation from triangular curve which indicates that the electrode materials have pseudocapacitive behavior. This behavior was due to reversible redox reactions. The current during these reactions is called faradic current. To charge and discharge completely $Ce_{0.55}Sn_{0.45}S_2$/NF materials took 999 seconds and 91 seconds respectively. The materials discharged fully because the total reactions occurred on the surface were not completely reversible. The decrease in discharging time may represent the irreversibility of the materials. In charging curve (upper curve) the peak represent oxidation and in discharging curve the peak is due to reduction. The deviation of the curve also justifies the cyclic voltammogram of the electrode.

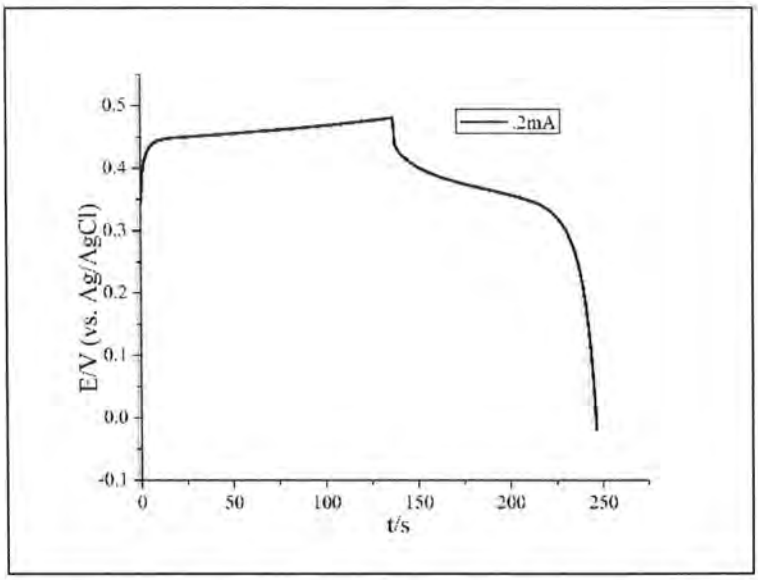

Figure 3.20 *GCD curves of the $Ce_{0.55}Sn_{0.45}S_2$/NF at 0.2Ag^{-1} current density*

3.7.3 Galvanostatic Charging/Discharging of GO

Figure 3.21 shows the charging and discharging of GO/NF supercapacitor in 0.1M KOH solution at constant current density ($2Ag^{-1}$). The procedure was same for galvanostatic charge and discharge as followed for cyclic voltammetry technique. figure 3.21 shows deviation from triangular curve which indicates that the electrode materials have pseudocapacitive behavior. This behavior was due to reversible redox reactions. The current during these reactions is called faradic current. To discharge completely GO/NF materials took 79 seconds. The materials discharged fully because the total reactions occurred on the surface were not completely reversible. The decrease in discharging time may represent the irreversibility of the materials. In charging curve (upper curve) the peak represent oxidation and in discharging curve the peak is due to reduction. The deviation of the curve also justifies the cyclic voltammogram of the electrode.

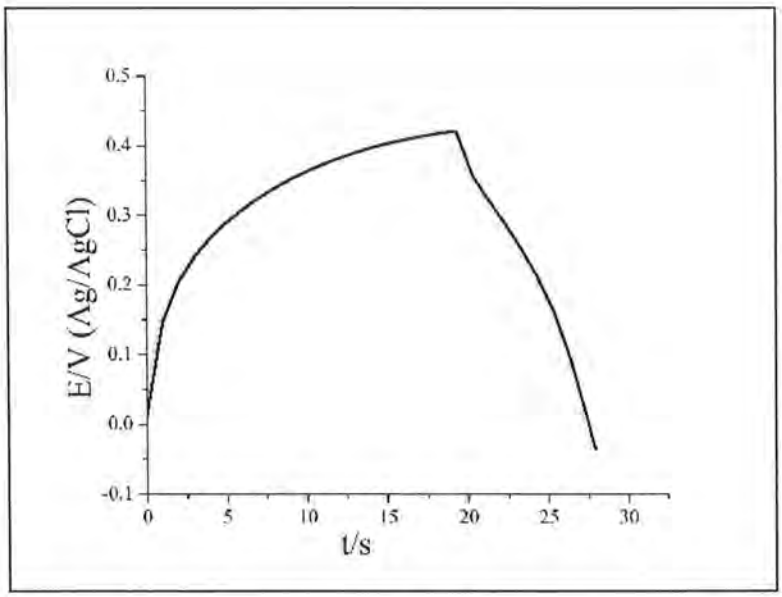

Figure 3.21 *GCD curves of the GO/NF at 0.2Ag^{-1} current density*

3.7.4 Galvanostatic Charging/Discharging of CeS_2/GO

Figure below shows the charging and discharging of CeS_2/GO/NF supercapacitor in 0.1M KOH solution at constant current density ($2Ag^{-1}$). The procedure was same for galvanostatic charge and discharge as followed for cyclic voltammetry technique. figure shows deviation from triangular curve which indicates that the electrode materials have pseudocapacitive behavior. This behavior was due to reversible redox reactions. The current during these reactions is called faradic current. To charge and discharge completely CeS_2/GO/NF materials took 998 seconds and 283 seconds respectively. The materials discharged fully because the total reactions occurred on the surface were not completely reversible. The decrease in discharging time may represent the irreversibility of the materials. In charging curve (upper curve) the peak represent oxidation and in discharging curve the peak is due to reduction. The deviation of the curve also justifies the cyclic voltammogram of the electrode.

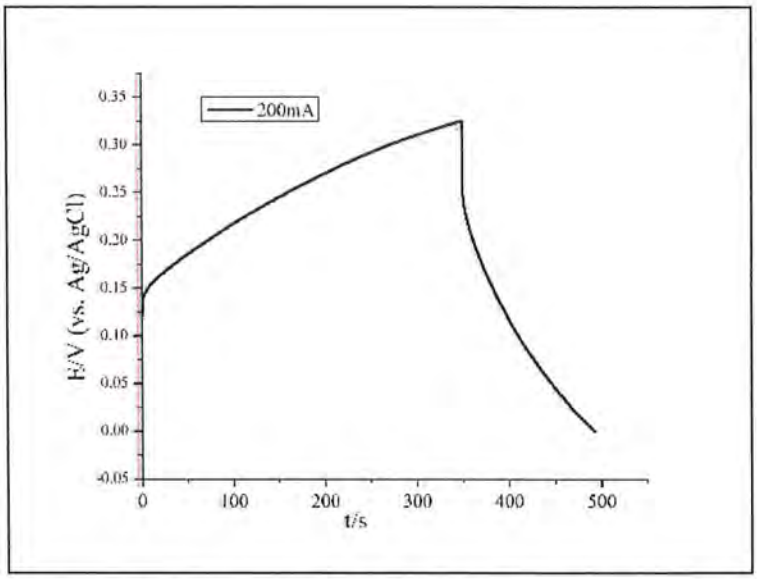

Figure 3.22 *GCD curves of the CeS_2/GO/NF at 0.2Ag^{-1} current density*

3.8 The effect of current density on GCD curve

3.8.1 The effect of Change in current density on GCD curve For CeS_2

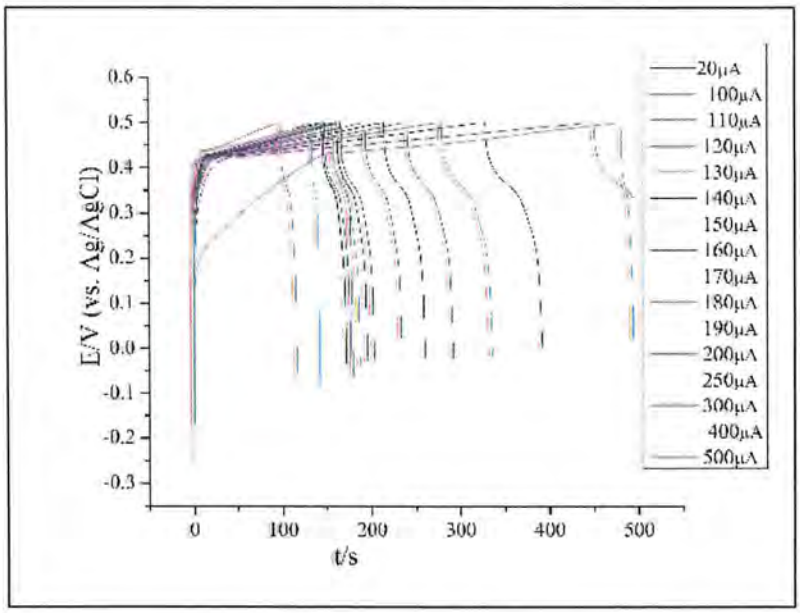

Figure 3.23 *GCD curves for CeS_2/NF at different current densities.*

Figure 3.23 Shows the galvanostatic charge and discharge curve for CeS_2/NiF at different current densities. the specific capacitances ware calculated as 128F/g, 127.3F/g,

127.2F/g, 120.6F/g and 117.6F/g at current densities of 0.2A/g, 1A/g, 1.1A/g, 1.2A/g and 1.3A/g, 1.4A/g, 1.5A/g respectively. These figures were calculated from GCD curves at different current densities. Specific capacitance of 128 F/g at current density of 0.2A/g was observed. It shows that the specific capacitance was decreased when current density was increased 3 times. The charging and discharging time were decreased for CeS_2/NF materials by changing the current densities. Specific capacitance calculated form CV and GCD Curves were closely matched to each other's. It was shown from the curve that the materials were nearer to capacitive behavior[81]. The figure 3.23 also indicates that the materials showed more nearer behavior to capacitive behavior at higher current density because of the control of diffusion.

3.8.2 The effect of Change in current density on GCD curve For $Ce_{0.55}Sn_{0.45}S_2$

Galvanostatic charge and discharge curve for $Ce_{0.55}Sn_{0.45}S_2$/NiF at different current densities **Figure 3.24**. GCD profile was used to calculate specific capacitances and values ware calculated by using different equation: 642F/g, 517.6F/g, 221.5F/g, 129.6F/g and 61F/g at current densities of 0.5A/g, 1A/g, 2A/g, 2.5A/g and 3A/g respectively. Among all specific capacitance the best result obtained for tin-doped cerium sulfide was 642 F/g at current density 0.5A/g was observed. The figure showed that when the current density increased the charging and discharging time decreased and it is due to more time is required to fully charge the electrode surface and we give burst of current density and it did not charge fully. It shows that the specific capacitance was decreased when current density was increased 3 times. The charging and discharging time were decreased for $Ce_{0.55}Sn_{0.45}S_2$/NF materials by changing the current densities (figure 3.24). The GCD curves deviated from ideal EDLCs and it is the further justification of cyclic voltammogram which showed two peaks. Specific capacitance calculated form CV and GCD Curves were closely matched to each other's. It was shown from the curve that the materials were nearer to capacitive behavior. This figure also indicates that the materials showed more nearer behavior to capacitive behaviour at higher current density because of the control of diffusion.

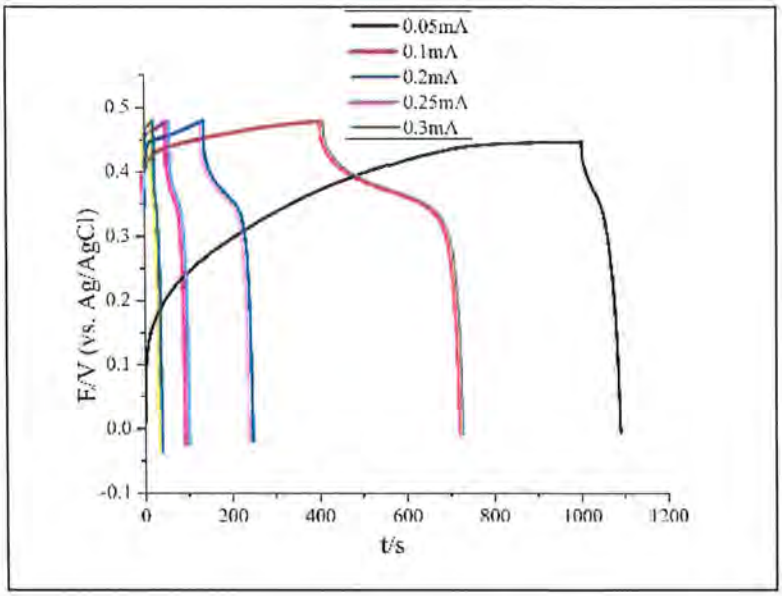

Figure 3.24 *GCD curves for $Ce_{0.55}Sn_{0.45}S_2$/NF at different current densities.*

3.8.3 The effect of Change in current density on GCD curve for GO

Figure 3.25 Shows the galvanostatic charge and discharge curve for GO/NF at different current densities. the specific capacitances ware calculated as 22.5F/g, 30F/g, 43F/g and 52F/g at current densities of 0.5A/g, 1A/g, 2A/g and 3A/g respectively. These figures were calculated from GCD curves at different current densities. It shows that the specific capacitance was decreased when current density was increased 3 times. The charging and discharging time were decreased for GO/NF materials by changing the current densities (figure 3.25). Specific capacitance calculated form CV and GCD Curves were closely matched to each other's. It was shown from the curve that the materials were nearer to capacitive behavior. The figure 3.25 also indicates that the materials showed more nearer behavior to capacitive behavior at higher current density because of the control of diffusion.

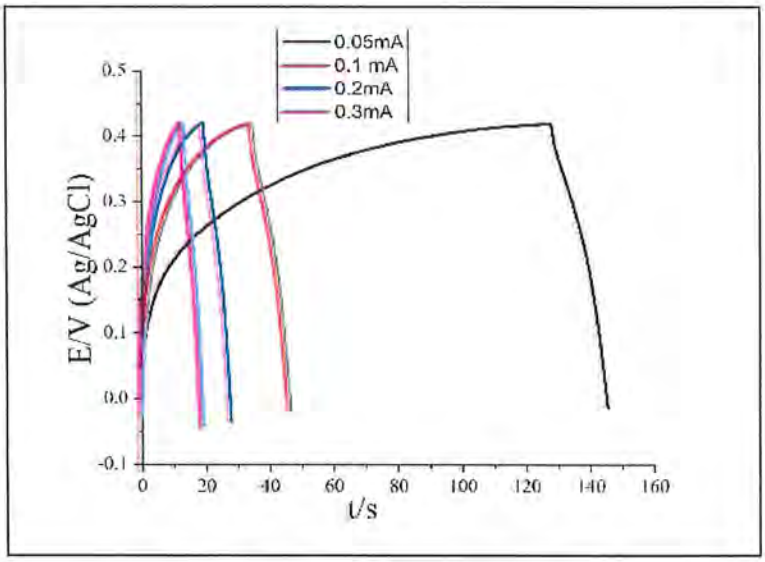

Figure 3.25 *GCD curves for GO/NF at different current densities.*

3.8.4 The effect of Change in current density on GCD curve for CeS_2/GO

To calculated power density and energy density the chronopotentiometry was performed and galvanostatic charge and discharge curve for CeS_2/GO/NiF at different current densities were obtained. By using different equations specific capacitances ware calculated as 808F/g, 608F/g, 468F/g and 342F/g at current densities of 1A/g, 1.5A/g, 2A/g and 2.5A/g respectively. In all specific capacitance the best specific capacitance of 808 F/g at current density of $1Ag^{-1}$ was observed. It showed that the specific capacitance was decreased when current density was increased, and it is due to the redox reaction occurs more time to complete. The charging and discharging time were decreased for CeS_2/GO/NF materials by changing the current densities (figure 3.26). Furthermore, the GCD curves deviated from electric double layer supercapacitor and it show two peaks and therefore it justified the CV. Specific capacitance calculated form CV and GCD curves were closely matched to each other's. It was shown from the curve that the materials were nearer to capacitive behavior at lower current density.

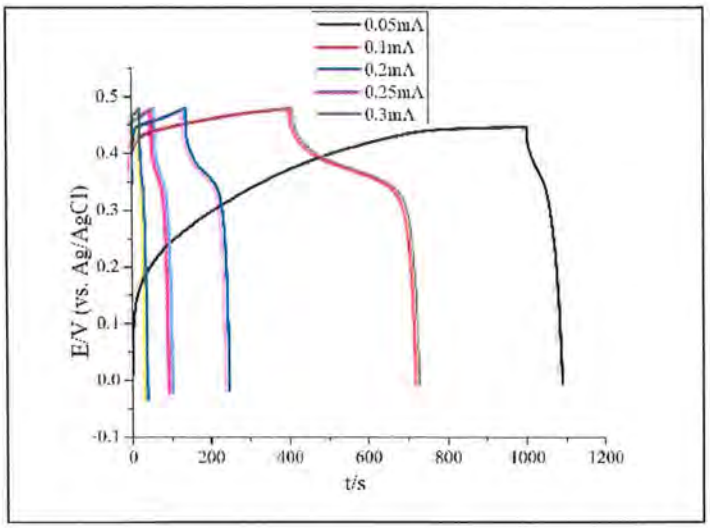

Figure 3.26 *Galvanostatic charging and discharging curves for CeS_2/GO/NF at different current densities.*

3.9 Energy density and Power density

3.9.1 Energy density and Power density of CeS2 nanoparticles

Power density and energy density of cerium Sulphide were determined from GCD curves. It was shown from the figure that energy density was decreased with increasing power density. Energy densities of 4.44 Wh/kg, 4.42 Wh/kg, 4.41 Wh/kg and 2.29 Wh/kg were calculated at power densities of 250 W/kg, 275 W/kg, 300 W/kg, and 325 W/kg respectively. Cerium Sulphide nanoparticles shown maximum energy density of 4.4 Wh/kg at power density of 250 W/kg. This plot is also called Ragone plot.

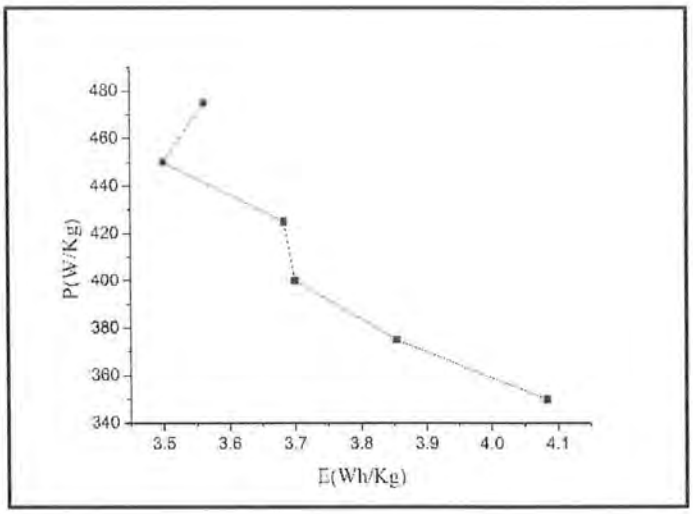

Figure 3.27 *Power density and Energy density of* CeS_2*/NF*

3.9.2 Energy density and Power density of $Ce_{0.55}Sn_{0.45}S_2$ nanoparticles

Galvanostatic charging discharging curves were used to calculate power density and energy density. Form the figure 2.28 it showed that the energy density and power density related inversely. Energy densities of 32.15Wh/kg, 25.2Wh/kg, 17.9Wh/kg, 7Wh/kg and 2.29Wh/kg were calculated at power densities of 1080W/kg, 1620W/kg, 2160W/kg, and 2700W/kg respectively. Tin-doped cerium sulfide showed the maximum energy density of 32.15Wh/Kg at power density of 100 W/Kg. This plot is also called Ragone plot.

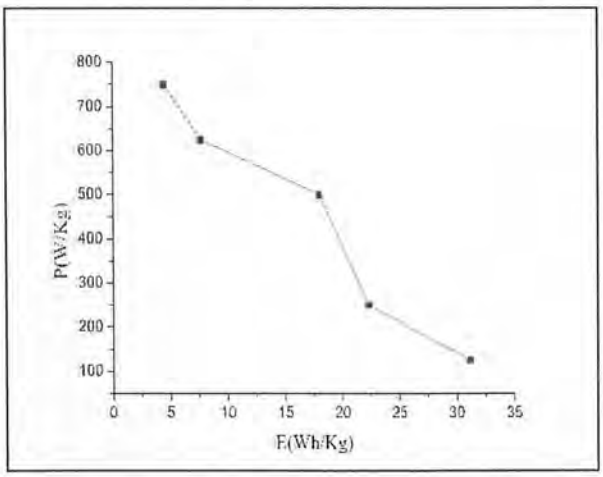

Figure 3.28 *Power density and Energy density of* $Ce_{0.55}Sn_{0.45}S_2$*/NF*

3.9.3 Energy density and Power density of CeS_2/GO nanoparticles

Power density and energy density of CeS_2/GO were determined from GCD curves. The figure indicated that energy density and power density was almost linearly inversely proportional to one another. Energy densities of 13.7Wh/kg, 10.3Wh/kg, 7.97Wh/kg, and 5.83Wh/kg were calculated at power densities of 175W/kg, 262W/kg, 350W/kg and 437.5W/kg respectively. CeS_2/GO nanoparticles shown maximum energy density of 13.7Wh/kg at power density of 175W/kg. The power density was plotted against energy density as shown in figure 2.29. It showed more better results than any other nanoparticles and nanocomposites, so it was better to use as supercapacitor.

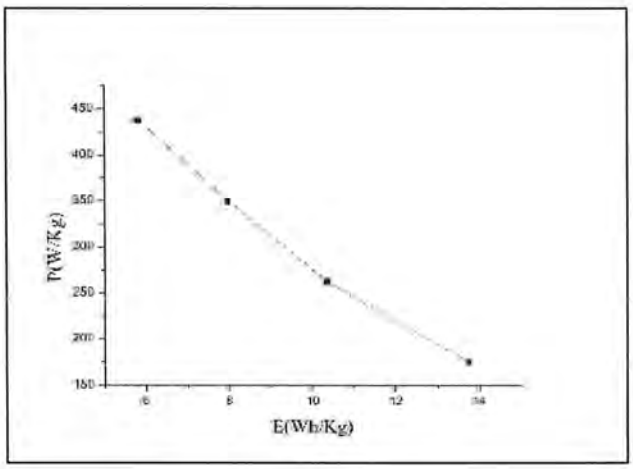

Figure 3.29 *Power density and Energy density of CeS_2/GO/NF*

Conclusion

GO was successfully synthesized by modified Hummer method. CeS_2, $Ce_{0.55}Sn_{0.45}S$ and their composite with GO were synthesized by hydrothermal process. XRD confirmed the phase purity of the materials. XRD pattern was compared with literature values. Which confirmed their successful synthesis. Their purity was also verified by FT-IR technique electrochemical studies of these materials were checked through cyclic voltammetry and Galvanostatic charge and discharge technique, the reaction on the surface of electrode material was found quasi reversible faradic reaction which indicated the pseudocapacitive behavior. The CV technique showed that current density was increased by increasing scan rate and justified that the materials were very stable and reversible. Even at 100mV/s the materials were stable and reversible. It may attribute to high conductivity of the materials. The oxidation and reduction peaks shifted at small potential when scan rate was increased. The GCD curve showed that the duration of charging and discharging decreased by increasing current density. CeS_2, $Ce_{0.55}Sn_{0.45}S$ and GO shown the highest specific capacitance of 426F/g, 436F/g and 1160F/g respectively at scan rate of 10mV/s. CeS_2/GO shown the highest specific capacitance of 690.4F/g at scan rate of 10 mV/s. It is concluded that, these materials have high values of specific capacitance at low scan rate and can be used as supercapacitors.

REFRENCES

1. Liu, A.; Jones, R.; Liao, L.; Samara-Rubio, D.; Rubin, D.; Cohen, O.; Nicolaescu, R.; Paniccia, M. A high-speed silicon optical modulator based on a metal–oxide–semiconductor capacitor. *Nat.* **2004,** *427* (6975), 615-618
2. Miller, J. R.; Simon, P. Electrochemical capacitors for energy management. *Sci. Mag.*, **2008,** *321* (5889), 651-652.
3. Teymourfar, R.; Asaei, B.; Iman-Eini, H. Stationary super-capacitor energy storage system to save regenerative braking energy in a metro line. *Energy Convers. Manag.*, **2012,** *56*, 206-214.
4. Díaz-González, F.; Sumper, A.; Gomis-Bellmunt, O.; Villafáfila-Robles, R. A review of energy storage technologies for wind power applications. *Renewable sustainable energy rev.*, **2012,** *16* (4), 2154-2171.
5. Friis, H. T. A note on a simple transmission formula. *Proce. IRE.*, **1946,** *34* (5), 254-256.
6. Wang, G.; Zhang, L.; Zhang, J. A review of electrode materials for electrochemical supercapacitors. *Chem. Soc. Rev.* **2012,** *41* (2), 797-828.
7. Zhi, M.; Xiang, C.; Li, J.; Li, M.; Wu, N. Nanostructured carbon–metal oxide composite electrodes for supercapacitors: a review. *Nanoscale* **2013,** *5* (1), 72-88.
8. Khan, M. A. R.; Rahaman, A. Ph.D thesis, *Development of nanocomposites for energy storage devices*, University of Texas at El Paso: 2012.
9. Lee, J.; Bartley, K. L.; Palusinski, O. A. Electrical characterization of nano structured energy storage devices. *ECS Transac.*, **2007,** *2* (8), 121-127.
10. Conway, B. E. Transition from "supercapacitor" to "battery" behavior in electrochemical energy storage. *J. Electrochem. Soc.*, **1991,** *138* (6), 1539-1548.
11. Conway, B.; Birss, V.; Wojtowicz, J. The role and utilization of pseudocapacitance for energy storage by supercapacitors, *J. Power Source,* **1997,** *66* (1-2), 1-14.
12. Qu, D. Studies of the activated carbons used in double-layer supercapacitors. *J. power source.*, **2002,** *109* (2), 403-411.
13. Bose, S.; Kuila, T.; Mishra, A. K.; Rajasekar, R.; Kim, N. H.; Lee, J. H. Carbon-based nanostructured materials and their composites as supercapacitor electrodes. *J. Mater. Chem.*, **2012,** *22* (3), 767-784.
14. Oh, S.; Kim, K. Synthesis of a new mesoporous carbon and its application to electrochemical double-layer capacitors. *Chem. Commun.*, **1999,** (21), 2177-2178.

15. Béguin, F.; Presser, V.; Balducci, A.; Frackowiak, E. Carbons and electrolytes for advanced supercapacitors. *Adv. mater.*, **2014,** *26* (14), 2219-2251.
16. Huang, Y.; Liang, J.; Chen, Y. An overview of the applications of graphene-based materials in supercapacitors. *Small* **2012,** *8* (12), 1805-1834.
17. Nikolaidis, P.; Poullikkas, A. A comparative review of electrical energy storage systems for better sustainability. *J. Power Techn.*, **2017,** *97* (3).
18. Brezesinski, T.; Wang, J.; Tolbert, S. H.; Dunn, B. Ordered mesoporous α-MoO 3 with iso-oriented nanocrystalline walls for thin-film pseudocapacitors. *Nat. Mater.*, **2010,** *9* (2), 146.
19. Ghosh, S.; Inganäs, O. Conducting polymer hydrogels as 3D electrodes: applications for supercapacitors. *Adv. Mater.*, **1999,** *11* (14), 1214-1218.
20. Barsukov, V.; Langouche, F.; Khomenko, V.; Makyeyeva, I.; Chernysh, O.; Gauthy, F. Modeling of porous graphite electrodes of hybride electrochemical capacitors and lithium-ion batteries. *J. Solid State Electrochem.*, **2015,** *19* (9), 2723-2732.
21. Benaouadj, M.; Aboubou, A.; Ayad, M.; Bahri, M.; Boucetta, A. In *Fuel cells, batteries and super-capacitors stand-alone power systems management using optimal/flatness based-control*, AIP Conference Proceedings, AIP Publishing: 2016; p 030022.
22. Vangari, M.; Pryor, T.; Jiang, L. Supercapacitors: review of materials and fabrication methods. *J. Energy Eng.*, **2012,** *139* (2), 72-79.
23. Yu, G.; Xie, X.; Pan, L.; Bao, Z.; Cui, Y. Hybrid nanostructured materials for high-performance electrochemical capacitors. *Nano Energy* **2013,** *2* (2), 213-234.
24. Licht, S.; Peramunage, D., Aluminum and sulfur electrochemical batteries and cells. Google Patents: **1995,** EP0677209A4.
25. Weir, R. D.; Nelson, C. W., Electrical-energy-storage unit (EESU) utilizing ceramic and integrated-circuit technologies for replacement of electrochemical batteries. Google Patents: **2009,** US7033406B2.
26. Kunduraci, M.; Al-Sharab, J. F.; Amatucci, G. G. High-Power Nanostructured LiMn2-x Ni x O4 High-Voltage Lithium-Ion Battery Electrode Materials: Electrochemical Impact of Electronic Conductivity and Morphology. *Chem. Mater.*, **2006,** *18* (15), 3585-3592.
27. Lozano-Castello, D.; Cazorla-Amorós, D.; Linares-Solano, A.; Shiraishi, S.; Kurihara, H.; Oya, A. Influence of pore structure and surface chemistry on electric double layer capacitance in non-aqueous electrolyte. *Carbon*, **2003,** *41* (9), 1765-1775.

28. Poizot, P.; Laruelle, S.; Grugeon, S.; Dupont, L.; Tarascon, J. Nano-sized transition-metal oxides as negative-electrode materials for lithium-ion batteries. *Nature,* **2000,** *407* (6803), 496.
29. Kim, S. W.; Seo, D. H.; Ma, X.; Ceder, G.; Kang, K. Electrode materials for rechargeable sodium-ion batteries: potential alternatives to current lithium-ion batteries. *Adv. Energy Mater.,* **2012,** *2* (7), 710-721.
30. Cui, L.-F.; Yang, Y.; Hsu, C.-M.; Cui, Y. Carbon– silicon core– shell nanowires as high capacity electrode for lithium ion batteries. *Nano Lett.,* **2009,** *9* (9), 3370-3374.
31. Voelker, P. Trace degradation analysis of lithium-ion battery components. *R&D Magazinde,(April 2014)* *http://www.rdmag.com/articles/2014/04/trace-degradation-analysislithium-ion-battery-components* **2014**.
32. Omar, N.; Daowd, M.; Bossche, P. v. d.; Hegazy, O.; Smekens, J.; Coosemans, T.; Mierlo, J. v. Rechargeable energy storage systems for plug-in hybrid electric vehicles Assessment of electrical characteristics. *Energies,* **2012,** *5* (8), 2952-2988.
33. Pushparaj, V. L.; Shaijumon, M. M.; Kumar, A.; Murugesan, S.; Ci, L.; Vajtai, R.; Linhardt, R. J.; Nalamasu, O.; Ajayan, P. M. Flexible energy storage devices based on nanocomposite paper. *Proce. National Academy Science.,* **2007,** *104* (34), 13574-13577.
34. Zheng, J.; Jow, T. High energy and high power density electrochemical capacitors. *J. Power Source.,* **1996,** *62* (2), 155-159.
35. Gao, X.; Klumperink, E. A.; Bohsali, M.; Nauta, B. A low noise sub-sampling PLL in which divider noise is eliminated and PD/CP noise is not multiplied by *IEEE J. Solid State Chem.,* **2009,** *44* (12), 3253-3263.
36. Li, W.; Joós, G.; Bélanger, J. Real-Time Simulation of a Wind Turbine Generator Coupled With a Battery Supercapacitor Energy Storage System. *IEEE Trans. Indus, Elec.,* **2010,** *57* (4), 1137-1145.
37. Luo, X.; Wang, J.; Dooner, M.; Clarke, J. Overview of current development in electrical energy storage technologies and the application potential in power system operation. *Appl. Energ.,* **2015,** *137,* 511-536.
38. Luo, X.; Morrin, A.; Killard, A. J.; Smyth, M. R. Application of nanoparticles in electrochemical sensors and biosensors. *Electroana.,* **2006,** *18* (4), 319-326.
39. Toshima, N.; Yonezawa, T. Bimetallic nanoparticles—novel materials for chemical and physical applications. *New J. Chem.,* **1998,** *22* (11), 1179-1201.

40. Hajipour, M. J.; Fromm, K. M.; Ashkarran, A. A.; de Aberasturi, D. J.; de Larramendi, I. R.; Rojo, T.; Serpooshan, V.; Parak, W. J.; Mahmoudi, M. Antibacterial properties of nanoparticles. *Trend biotechnol.*, **2012,** *30* (10), 499-511.
41. Choi, H.; Veriansyah, B.; Kim, J.; Kim, J.-D.; Kang, J. W. Continuous synthesis of metal nanoparticles in supercritical methanol. *J. Supercriti. Fluid.*, **2010,** *52* (3), 285-291.
42. Brust, M.; Walker, M.; Bethell, D.; Schiffrin, D. J.; Whyman, R. Synthesis of thiol-derivatised gold nanoparticles in a two-phase liquid–liquid system. *J. ACS. Chem. Commun.*, **1994,** (7), 801-802.
43. Pottier, A.; Cassaignon, S.; Chanéac, C.; Villain, F.; Tronc, E.; Jolivet, J.-P. Size tailoring of TiO 2 anatase nanoparticles in aqueous medium and synthesis of nanocomposites. Characterization by Raman spectroscopy. *J. Mater. Chem.*, **2003,** *13* (4), 877-882.
44. Zhang, Z.; Chen, D. Consideration of Orowan strengthening effect in particulate-reinforced metal matrix nanocomposites: A model for predicting their yield strength. *Scripta Materialia,* **2006,** *54* (7), 1321-1326.
45. Moniruzzaman, M.; Winey, K. I. Polymer nanocomposites containing carbon nanotubes. *Macromole.*, **2006,** *39* (16), 5194-5205.
46. Song, Y. S.; Youn, J. R. Influence of dispersion states of carbon nanotubes on physical properties of epoxy nanocomposites. *Carbon,* **2005,** *43* (7), 1378-1385.
47. Gao, G.; Cagin, T.; Goddard III, W. A. Energetics, structure, mechanical and vibrational properties of single-walled carbon nanotubes. *Nanotech.*, **1998,** *9* (3), 184.
48. Colvin, V.; Goldstein, A.; Alivisatos, A. Semiconductor nanocrystals covalently bound to metal surfaces with self-assembled monolayers. *J. ACS.*, **1992,** *114* (13), 5221-5230.
49. Zhu, T.; Wang, Z.; Ding, S.; Chen, J. S.; Lou, X. W. D. Hierarchical nickel sulfide hollow spheres for high performance supercapacitors. *Rsc Adv.*, **2011,** *1* (3), 397-400.
50. Yu, L.; Zhang, L.; Wu, H. B.; Lou, X. W. Formation of NixCo3− xS4 hollow nanoprisms with enhanced pseudocapacitive properties. *Ange. Chemie. Inter. Ed.* **2014,** *53* (14), 3711-3714.
51. Rahman, M. M.; Ahmed, J.; Asiri, A. M. A glassy carbon electrode modified with γ-Ce 2 S 3-decorated CNT nanocomposites for uric acid sensor development: a real sample analysis. *RSC Adv.*, **2017,** *7* (24), 14649-14659.

52. Zhang, J.; Zhao, X. Conducting polymers directly coated on reduced graphene oxide sheets as high-performance supercapacitor electrodes. *J. Phys. Chem. C* **2012,** *116* (9), 5420-5426.
53. Bibi, N.; Xia, Y.; Ahmed, S.; Zhu, Y.; Zhang, S.; Iqbal, A. Highly stable mesoporous CeO2/CeS2 nanocomposite as electrode material with improved supercapacitor electrochemical performance. *Ceram. Interl,* **2018,** *44* (18), 22262-22270.
54. Raj, D. V.; Raj, C. J.; Das, S. J. Synthesis and optical properties of cerium doped zinc sulfide nano particles. *Superlattices and Microstructures* **2015,** *85*, 274-281.
55. Marcano, D. C.; Kosynkin, D. V.; Berlin, J. M.; Sinitskii, A.; Sun, Z.; Slesarev, A.; Alemany, L. B.; Lu, W.; Tour, J. M. Improved synthesis of graphene oxide. *ACS nano* **2010,** *4* (8), 4806-4814.
56. Stankovich, S.; Dikin, D. A.; Piner, R. D.; Kohlhaas, K. A.; Kleinhammes, A.; Jia, Y.; Wu, Y.; Nguyen, S. T.; Ruoff, R. S. Synthesis of graphene-based nanosheets via chemical reduction of exfoliated graphite oxide. *carbon,* **2007,** *45* (7), 1558-1565.
57. Compton, O. C.; Nguyen, S. T. Graphene oxide, highly reduced graphene oxide, and graphene: versatile building blocks for carbon-based materials. *Small,* **2010,** *6* (6), 711-723.
58. Wang, G.; Huang, J.; Chen, S.; Gao, Y.; Cao, D. Preparation and supercapacitance of CuO nanosheet arrays grown on nickel foam. *J. Power Source.,* **2011,** *196* (13), 5756-5760.
59. Gomes Silva, C. u.; Juárez, R.; Marino, T.; Molinari, R.; García, H. Influence of excitation wavelength (UV or visible light) on the photocatalytic activity of titania containing gold nanoparticles for the generation of hydrogen or oxygen from water. *J. ACS.,* **2010,** *133* (3), 595-602.
60. Kowalska, E.; Mahaney, O. O. P.; Abe, R.; Ohtani, B. Visible-light-induced photocatalysis through surface plasmon excitation of gold on titania surfaces. *Phys. Chem. Chem. Phys.,* **2010,** *12* (10), 2344-2355.
61. Swinehart, D. The beer-lambert law. *J. Chem. Edu.* **1962,** *39* (7), 333.
62. Nicholson, R. S. Theory and application of cyclic voltammetry for measurement of electrode reaction kinetics. *Anal. Chemistry* **1965,** *37* (11), 1351-1355.
63. Kissinger, P. T.; Heineman, W. R. Cyclic voltammetry. *J. Chem. Edu.* **1983,** *60* (9), 702.
64. Wang, H.; Cao, G.; Prior, R. L. Oxygen radical absorbing capacity of anthocyanins. *J. agri. Food Chem.,* **1997,** *45* (2), 304-309.

65. Clausen, B. S. Combined (Q) EXAFS/XRD: Technique and applications. *Catal. Today.*, **1998,** *39* (4), 293-300.

66. Birks, L.; Friedman, H. Particle size determination from X-ray line broadening. *J. Appl. Phys.*, **1946,** *17* (8), 687-692.

67. Cen, H.; He, Y. Theory and application of near infrared reflectance spectroscopy in determination of food quality. *Trends Food Sci. Tech.* **2007,** *18* (2), 72-83.

68. Chen, Z.; Liu, S.; Yang, M.-Q.; Xu, Y.-J. Synthesis of uniform CdS nanospheres/graphene hybrid nanocomposites and their application as visible light photocatalyst for selective reduction of nitro organics in water. *ACS Appl. Mater. Interfaces.*, **2013,** *5* (10), p4309-4319.

69. Alam, S. N.; Sharma, N.; Kumar, L. Synthesis of graphene oxide (GO) by modified hummers method and its thermal reduction to obtain reduced graphene oxide (rGO). *Graphene*, **2017,** *6* (01), 1.

70. Zhang, L.; Li, Y.; Zhang, L.; Li, D.-W.; Karpuzov, D.; Long, Y.-T. Electrocatalytic oxidation of NADH on graphene oxide and reduced graphene oxide modified screen-printed electrode. *Int. J. Electrochem. Sci.*, **2011,** *6* (3), 819-829.

71. Zhang, Y.; Li, H.; Pan, L.; Lu, T.; Sun, Z. Capacitive behavior of graphene–ZnO composite film for supercapacitors. *J. Electroana. Chem.*, **2009,** *634* (1), 68-71.

72. Yan, J.; Fan, Z.; Wei, T.; Qian, W.; Zhang, M.; Wei, F. Fast and reversible surface redox reaction of graphene–MnO2 composites as supercapacitor electrodes. *Carbon,* **2010,** *48* (13), 3825-3833.

73. Xu, B.; Wu, F.; Su, Y.; Cao, G.; Chen, S.; Zhou, Z.; Yang, Y. Competitive effect of KOH activation on the electrochemical performances of carbon nanotubes for EDLC: balance between porosity and conductivity. *Electrochim. Acta.*, **2008,** *53* (26), 7730-7735.

74. Gryglewicz, G.; Machnikowski, J.; Lorenc-Grabowska, E.; Lota, G.; Frackowiak, E. Effect of pore size distribution of coal-based activated carbons on double layer capacitance. *Electrochim. Acta.*, **2005,** *50* (5), 1197-1206.

75. Yan, J.; Fan, Z.; Sun, W.; Ning, G.; Wei, T.; Zhang, Q.; Zhang, R.; Zhi, L.; Wei, F. Advanced asymmetric supercapacitors based on Ni (OH) 2/graphene and porous graphene electrodes with high energy density. *Adv. Fun. Mater.*, **2012,** *22* (12), 2632-2641.

76. Vivekchand, S.; Rout, C. S.; Subrahmanyam, K.; Govindaraj, A.; Rao, C. Graphene-based electrochemical supercapacitors. *J. Chem. Sci.*, **2008,** *120* (1), 9-13.

77. Chen, J.; Xia, Z.; Li, H.; Li, Q.; Zhang, Y. Preparation of highly capacitive polyaniline/black TiO2 nanotubes as supercapacitor electrode by hydrogenation and electrochemical deposition. *Electrochim. Acta.*, **2015,** *166*, 174-182.